

SECURITY CLASSIFICATION OF THIS PAGE (When Data Entered)

REPORT DOCUMENTATION PAGE		READ INSTRUCTIONS BEFORE COMPLETING FORM	
1. REPORT NUMBER NAVENVPREDRSCHFAC Technical Report TR 80-08	2. GOVT ACCESSION NO.	3. RECIPIENT'S CATALOG NUMBER	
4. TITLE (and Subtitle) An Automatic Cloud Tracking System Based on the Cross-Covariance Method		5. TYPE OF REPORT & PERIOD COVERED Final	
		6. PERFORMING ORG. REPORT NUMBER TR 80-08	
7. AUTHOR(s) David H. Lee and Roland E. Nagle		8. CONTRACT OR GRANT NUMBER(s)	
9. PERFORMING ORGANIZATION NAME AND ADDRESS Naval Environmental Prediction Research Facility Monterey, California 93940		10. PROGRAM ELEMENT, PROJECT, TASK AREA & WORK UNIT NUMBERS PE 62759N, PN 9F52551792 NEPRF WU 6.2-12	
11. CONTROLLING OFFICE NAME AND ADDRESS Naval Air Systems Command Department of the Navy Washington, DC 20361		12. REPORT DATE December 1980	
		13. NUMBER OF PAGES 64	
14. MONITORING AGENCY NAME & ADDRESS (if different from Controlling Office)		15. SECURITY CLASS. (of this report) UNCLASSIFIED	
		15a. DECLASSIFICATION/DOWNGRADING SCHEDULE	
16. DISTRIBUTION STATEMENT (of this Report) Approved for public release; distribution unlimited			
17. DISTRIBUTION STATEMENT (of the abstract entered in Block 20, if different from Report)			
18. SUPPLEMENTARY NOTES Original manuscript received in August 1980.			
19. KEY WORDS (Continue on reverse side if necessary and identify by block number) Satellite winds Quantitative satellite information Satellite cloud tracking Cloud motion vectors Cloud winds Cross-covariance GOES			
20. ABSTRACT (Continue on reverse side if necessary and identify by block number) An automatic cloud tracking system based on the computation of the cross-covariance between satellite images has been developed. The six steps of the System for Automatic Wind Extraction from Geostationary Satellite-Data (SAWEGS) are preprocessing, cloud tracking, height assignment, earth location, wind vector computation, and quality control. The system embodies various unique aspects developed to address the problems encountered with an automated technique in general and this technique in particular. (Continued on reverse)			

Block 20, Abstract, Continued

These aspects include histogram-based temperature slicing, cloud edge and surface enhancement, tracking trackability tests, and use of numerical analysis temperature profiles for height assignment. Examples of applying SAWEGS to visible data, to infrared data, and to a difficult tropical cyclone case show the good quality and coverage of resulting vectors as well as the remaining difficulties.

AN (1) AD-A098 124
 FG (2) 040200
 FG (2) 170500
 CI (3) (U)
 CA (5) NAVAL ENVIRONMENTAL PREDICTION RESEARCH FACILITY
 MONTEREY CA
 TI (6) An Automatic Cloud Tracking System Based on the
 Cross-Covariance Method.
 TC (8) (U)
 DN (9) Final rept.,
 AU (10) Lee, David H.
 AU (10) Nagle, Roland E.
 RD (11) Dec 1980
 PG (12) 65p
 RS (14) NEPRF-TR-80-08
 PJ (16) F52551
 TN (17) WF52551792
 RC (20) Unclassified report
 DE (23) *Clouds, *Tracking, Automatic, Artificial satellites,
 Optical images, Image processing, Cross correlation,
 Covariance, Histograms, Motion, Height
 DC (24) (U)
 ID (25) *SAWEGS(System for Automatic Wind Extraction from
 Geostationary Satellite Data), Cross covariance,
 Histogram slicing, Satellite image measurement,
 PE62759N, WU6212
 IC (26) (U)
 AB (27) An automatic cloud tracking system based on the
 computation of the cross-covariance between satellite
 images has been developed. The six steps of the System
 for Automatic Wind Extraction from Geostationary
 Satellite-Data (SAWEGS) are preprocessing, cloud
 tracking, height assignment, earth location, wind
 vector computation, and quality control. The system
 embodies various unique aspects developed to address
 the problems encountered with an automated technique in
 general and this technique in particular. These aspects
 include histogram-based temperature slicing, cloud edge
 and surface enhancement, tracking trackability tests,
 and use of numerical analysis temperature profiles for
 height assignment. Examples of applying SAWEGS to
 visible data, to infrared data, and to a difficult
 tropical cyclone case show the good quality and
 coverage of resulting vectors as well as the remaining
 difficulties. (Author)
 AC (28) (U)
 DL (33) 01
 SE (34) F
 CC (35) 407279

ROUTINE REPLY, ENDORSEMENT, TRANSMITTAL OR INFORMATION SHEET

OPNAV 5216/158 (Rev. 7 78)

A WINDOW ENVELOPE MAY BE USED

SN 0107 LF 052-1691

Formerly NAVEXOS 3789

CLASSIFICATION (UNCLASSIFIED when detached from enclosures, unless otherwise indicated)

UNCLASSIFIED

FROM (Show telephone number in addition to address)

 Commanding Officer, Naval Environmental Prediction Research
 Facility, Monterey, CA 93940 AVN 878-2928

DATE

2 MAR 1981

SUBJECT

NAVENVPREDRSCHFAC technical publications; forwarding of

SERIAL OR FILE NO.

NEPRF/SBB:sb 5600

SER: 106

TO:

REFERENCE

Distribution

[See end pages, enclosures (1), (2)]

ENCLOSURE

 (1) NAVENVPREDRSCHFAC
 Technical Report TR 80-08:
 An Automatic Cloud Tracking
 System Based On The Cross-
 Covariance Method
 (2) NAVENVPREDRSCHFAC
 Contractor Report CR 80-05:
 Satellite Wind-Profile
 Techniques

VIA:

ENDORSEMENT ON

☒ FORWARDED ☐ RETURNED ☐ FOLLOW-UP, OR TRACER ☐ REQUEST ☐ SUBMIT ☐ CERTIFY ☐ MAIL ☐ FILE

GENERAL ADMINISTRATION		CONTRACT ADMINISTRATION		PERSONNEL	
FOR APPROPRIATE ACTION		NAME & LOCATION OF SUPPLIER OF SUBJECT ITEMS		REPORTED TO THIS COMMAND:	
UNDER YOUR COGNIZANCE		SUBCONTRACT NO. OF SUBJECT ITEM			
XX INFORMATION & retention APPROVAL RECOMMENDED <input type="checkbox"/> YES <input type="checkbox"/> NO		APPROPRIATION SYMBOL, SUBHEAD, AND CHARGEABLE ACTIVITY		DETACHED FROM THIS COMMAND	
<input type="checkbox"/> APPROVED <input type="checkbox"/> DISAPPROVED		SHIPPING AT GOVERNMENT EXPENSE <input type="checkbox"/> YES <input type="checkbox"/> NO		OTHER	
COMMENT AND/OR CONCURRENCE		A CERTIFICATE, VICE BILL OF LADING			
CONCUR		COPIES OF CHANGE ORDERS, AMENDMENT OR MODIFICATION			
LOANED, RETURN BY:		CHANGE NOTICE TO SUPPLIER			
SIGN RECEIPT & RETURN		STATUS OF MATERIAL ON PURCHASE DOCUMENT			
REPLY TO THE ABOVE BY:					
REFERENCE NOT RECEIVED		REMARKS (Continue on reverse)			
SUBJECT DOCUMENT FORWARDED TO:		Enclosure (1) describes an automatic cloud tracking system based on the computation of the cross-covariance between satellite images, and gives examples of this system's application. Enclosure (2) presents the results of a study to investigate techniques of deriving wind profiles from cloud motion vectors and satellite temperature soundings; a selected number of techniques are tested and compared.			
SUBJECT DOCUMENT RETURNED FOR					
SUBJECT DOCUMENT HAS BEEN REQUESTED, AND WILL BE FORWARDED WHEN RECEIVED					
COPY OF THIS CORRESPONDENCE WITH YOUR REPLY					
ENCLOSURE NOT RECEIVED					
ENCLOSURE FORWARDED AS REQUESTED					
ENCLOSURE RETURNED FOR CORRECTION AS INDICATED					
CORRECTED ENCLOSURE AS REQUESTED					
REMOVE FROM DISTRIBUTION LIST					
REDUCE DISTRIBUTION AMOUNT TO					
SIGNATURE & TITLE		Commanding Officer			

COPY TO:

CLASSIFICATION (UNCLASSIFIED when detached from enclosures, unless otherwise indicated)

UNCLASSIFIED



LIBRARY
RESEARCH REPORTS DIVISION
NAVAL POSTGRADUATE SCHOOL
MONTEREY, CALIFORNIA 93940

**NAVENVPREDRSCHFAC
TECHNICAL REPORT
TR-80-08**

NAVENVPREDRSCHFAC TR 80-08

AN AUTOMATIC CLOUD TRACKING SYSTEM BASED ON THE CROSS-COVARIANCE METHOD

David H. Lee and Roland E. Nagle
Naval Environmental Prediction Research Facility

DECEMBER 1980

APPROVED FOR PUBLIC RELEASE
DISTRIBUTION UNLIMITED



**NAVAL ENVIRONMENTAL PREDICTION RESEARCH FACILITY,
MONTEREY, CALIFORNIA 93940**

QUALIFIED REQUESTORS MAY OBTAIN ADDITIONAL COPIES
FROM THE DEFENSE TECHNICAL INFORMATION CENTER.
ALL OTHERS SHOULD APPLY TO THE NATIONAL TECHNICAL
INFORMATION SERVICE.

CONTENTS

1.	INTRODUCTION	1
2.	BACKGROUND	3
2.1	Automatic Cloud Tracking Systems	3
2.2	The Cross-Covariance Method	5
3.	SAWEGS	7
3.1	Preprocessing	7
3.1.1	Image Partitioning	7
3.1.2	Histogram Slicing	7
3.1.3	Edge and Pattern Enhancement	13
3.2	Cloud Tracking	18
3.2.1	The XCOV Method	18
3.2.2	XCOV Matrix Origin Determination	18
3.2.3	No-Tracking Tests	21
3.3	Height Assignment	22
3.4	Earth Location and Wind Vector Computation	22
3.5	Quality Control	24
4.	APPLICATION RESULTS	27
4.1	Infrared	27
4.2	Visible	32
4.3	Tropical Cyclone	33
4.4	Effect of Subarea Size	37
5.	DISCUSSION AND CONCLUSIONS	45
6.	CONTINUED DEVELOPMENT	49
	REFERENCES	51
	APPENDIX A: SLICING TECHNIQUE EVOLUTION	53
	APPENDIX B: XCOV MATRIX ORIGIN DETERMINATION DEVELOPMENT	55
	DISTRIBUTION	57

1. INTRODUCTION

Winds derived by tracking the motion of clouds in consecutive geostationary satellite images are important in correctly portraying the atmospheric state over the oceans and over other regions where only limited data from other sources are available. Unfortunately, most systems for deriving these winds still require a substantial human contribution, usually in selecting the clouds to be tracked and in monitoring the quality of resultant vectors. In an operational environment, this sizable commitment of personnel is undesirable. Furthermore, Leese et al. (1971) found a strong bias in the speeds of operational, manually-tracked cloud motion vectors toward the mid-range, a characteristic not found in winds tracked in a non-operational mode. They attributed this to the pressures of deadlines evident in an operational environment.

Automatic, computer-based cloud tracking systems do not have these problems. Automatic systems produce fields of cloud motion vectors in a fraction of the time necessary for manual tracking and, since the tracking is performed by some repeatable algorithm, the system is inherently objective.

However, automatic systems cannot as yet generate the quality of winds produced by manual tracking in a research environment. The development of automatic systems involves other challenges as well. But for operational applications, automatic cloud tracking has the optimum balance of efficiency and quality.

This report describes the development of an automatic cloud-tracking system based on the cross-covariance method. Following a general discussion of automatic tracking, the development of the Navy System for Automatic Wind Extraction from Geostationary Satellite-Data (SAWEGS) is described, and examples of its application are discussed.

2. BACKGROUND

2.1 AUTOMATIC CLOUD TRACKING SYSTEMS

Two automatic cloud tracking systems were developed nearly a decade ago; these are a cross-correlation system now used operationally for low level winds by the National Oceanic and Atmospheric Administration's (NOAA) National Environmental Satellite Service (Leese et al., 1971; Green et al., 1975; Novak and Young, 1977) and a technique using pattern recognition developed by SRI International (Endlich et al., 1971; Wolf et al., 1977; Wolf and Endlich, 1980).

Other systems are currently being developed. One is based on an existing automatic precipitation forecasting program at McGill University in Montreal, Quebec, Canada (Austin and Bellon, 1979; Bellon and Austin, 1978; Austin, 1980). The European Space Agency (ESA) is developing a system for operational use with the METEOSAT Satellite (Bizzarri and Tomassini, 1976; European Space Agency, 1978). Another system based on a method called "template tracking" is in preliminary stages of development by the Marshall Space Flight Center Atmospheric Sciences Division (Wilson, 1980). The authors are aware of no other automatic cloud tracking procedures.

The NESS, ESA, and McGill systems all use the cross-correlation method. This method identifies cloud displacements by determining all possible correlations between a target array and a larger comparison search array. The displacement of the target array giving the maximum correlation identifies the cloud motion vector. The NESS system uses a 32x32 target array and a 64x64 search array. Although used operationally for low level vectors, the system has not been deemed satisfactory for use at higher levels; at these levels manual tracking is still used.

Clouds at all levels are tracked using the ESA automatic wind extraction system. This system includes the use of bi-dimensional histograms for identifying tracers, a two-step tracking procedure using the infrared and visible data, and the use of the METEOSAT 6.7 μm "water vapor" channel in height assignment (Hubert, 1979; Bowen et al., 1980; Tomassini, 1980).

The McGill system has given good results with radar data for precipitation forecasting, but is still being developed for application to the more complex problems of cloud tracking (Austin, 1980).

The SRI system uses a different approach called "clustering," identifying groups of image brightness points that represent clouds. The program first locates points that have the greatest deviation in brightness from the mean of surrounding points, then groups them using a pattern recognition technique. Clusters within successive images are matched based on a computed "fit factor" to produce the cloud motion vector.

2.2 THE CROSS-COVARIANCE METHOD

SAWEGS, the System for Automatic Wind Extraction from Geostationary Satellite-Data, is based on computation of a cross-covariance (XCOV) between two satellite images. Although Leese et al. (1971) alluded to XCOV values as a by-product of the cross-correlation method and described the use of the Fast Fourier Transform (FFT) for computing the cross-correlation, Weinstein (1972) first realized that displacement information about the original images is related to a FFT-produced cross-covariance function directly. The fact that the maximum value of the XCOV matrix defines the major image-to-image displacement is the key to the XCOV method.

Arking et al. (1978) performed a set of limited experiments with a cross-covariance cloud tracking algorithm. They concluded that this technique produces good motion estimates, but is sensitive to situations in which a mixture of motions are present. Mixed motion cases are, of course, difficult to track for all cloud tracking systems, including manual systems (Hubert, 1979).

The cross-correlation and XCOV methods are often mistakenly assumed to be identical since, in a statistical sense, the cross-correlation is the XCOV divided by the product of the root-mean-squared variations of the input images. But as cloud tracking methods, they are different. In the cross-correlation method, a separate cross-correlation calculation must be made for each comparison of the target area with all possible alignments in the larger search area. The displacement is then derived from this set of correlations. In the XCOV method the displacement is a direct result of the single XCOV computation.

As with any automatic cloud tracking technique, problems exist with the XCOV method. If two or more different cloud motions are evident in a subarea, the XCOV operation tends to cancel these motions one against the other and to produce a displacement that does not accurately represent any motion. The XCOV method also attempts to determine one vector in each NxN subarea; therefore, to avoid producing meaningless vectors, a determination must be made

as to whether or not each subarea contains "trackable" cloud motions, i.e., motions from subareas in which clouds are evident. The location within the subarea to which the resulting vector is assigned must also be determined. Height assignment, a problem in all cloud tracking procedures, becomes more complex because the count value¹ on which to base the assignment is not a result of the tracking process. Because of the cyclic nature of the FFT, functions in the space domain are periodic. This results in an $N \times N$ XCOV matrix which represents both positive and negative displacements and, thus, all four quadrants of an equivalent $2N \times 2N$ matrix; therefore, there is an ambiguity in the matrix origin from which to locate the displacement.

¹"Count" is a satellite term which refers to the value of the radiation sensed at one image location, quantized over the full range of bits, e.g., eight bits for infrared and six bits for visible data. Count is directly equivalent to a brightness value for visible data and to temperature for infrared data.

3. SAWEGS

The System for Automatic Wind Extraction from Geostationary Satellite Data (SAWEGS) consists of six basic steps:

- 1) preprocessing
- 2) XCOV cloud tracking
- 3) height assignment
- 4) earth location
- 5) wind vector computation
- 6) quality control

Each of these steps will be discussed in detail in this section; they are portrayed schematically in Figure 1.

3.1 PREPROCESSING

3.1.1 Image Partitioning

SAWEGS operates on two 512 line by 512 element arrays of image counts from the same portion of two successive geostationary satellite images. Either visible or infrared data may be used. These images are divided into $N \times N$ subareas; one cloud motion vector results from each subarea containing trackable cloud elements. This subarea size should be a power of two for efficient utilization of the FFT. For a 30 minute interval (the operational time interval between successive GOES satellite images) and 8 km image resolution, a 32×32 subarea size was found to be most effective.

3.1.2 Histogram Slicing

One method of separating the multiple cloud motions which may exist in a subarea is to "slice" the 2-dimensional distribution of counts into regions, each with a different range of counts. These counts roughly correspond to cloud height in infrared data and to a combination of cloud thickness and height in visible data. SAWEGS analyzes the frequency distribution of count values to determine the limits of the slice within a subarea. The dynamic range of counts (0 to 256 for 8-bit data) is divided into 32 categories of eight values each. A subarea's frequency of

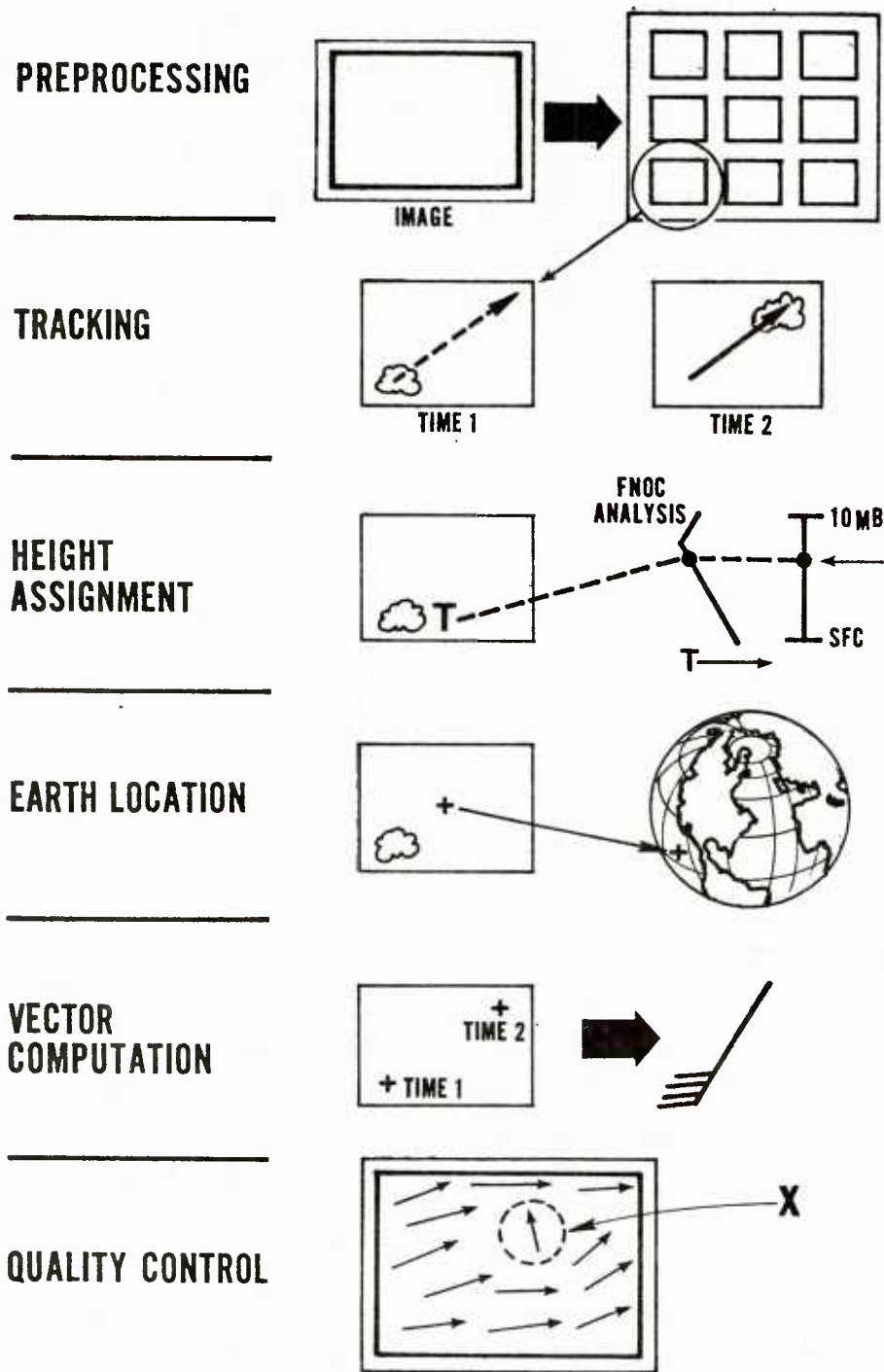


Figure 1. Schematic representation of the six basic steps in the System for Automatic Wind Extraction from Geostationary Satellite Data. Preprocessing involves partitioning the image, vertical slicing of the data, and enhancement of patterns and cloud edges. Tracking is applied to each individual subarea of the image, a height assigned using Fleet Numerical Oceanography Center (FNOC) temperature analyses, the position in image coordinates earth located, and the wind speed and direction computed. A quality control procedure is applied for the entire image after all vectors are produced."

occurrence histogram over these 32 categories reveals the dominant count range existing in the subarea. Cloud elements with a count value in this range comprise the cloud the system will track.

Various types and mixtures of clouds produce different characteristic frequency distributions. In the infrared, if most of the area within a subarea is covered by land or ocean surface, histogram spikes appear at very low count categories (high temperature). Low, middle, and high clouds show maximum frequency of occurrences at respectively higher count values (lower temperatures). Multiple cloud layers or clouds and surface occurring in the same subarea produce multiple peaks in the histogram distribution. Mixtures of many levels of clouds can produce a nearly level distribution across many categories. Characteristic histograms for each of these situations are shown in Figure 2. Enlargements of the infrared image subareas corresponding to these histograms are shown in Figure 3.

Only one slice per subarea is identified for tracking. Since the major cloud features in a subarea are identified by the maximum peak in the frequency distribution, the count range of the slice is defined as the count values between the local minimum on either side of the histogram peak.

By removing insignificant peaks and valleys, the distribution is first smoothed; this smoothing aids in discrimination of histogram maxima and minima. The smoothing algorithm used for this purpose is

$$X_n' = X_n - 0.4 [X_n - (X_{n-2} + 3X_{n-1} + 3X_{n+1} + X_{n+2})/8],$$

where X_n is the number of image counts in category n before smoothing, and X_n' is the corresponding smoothed value. Since the purpose for smoothing is the identification of extrema, not their absolute magnitudes, this algorithm was designed to be a radical smoother. Most minor variations in the distribution are removed, yet major peaks and valleys are maintained. Because this algorithm tends to increase the extent of the distribution, a check during

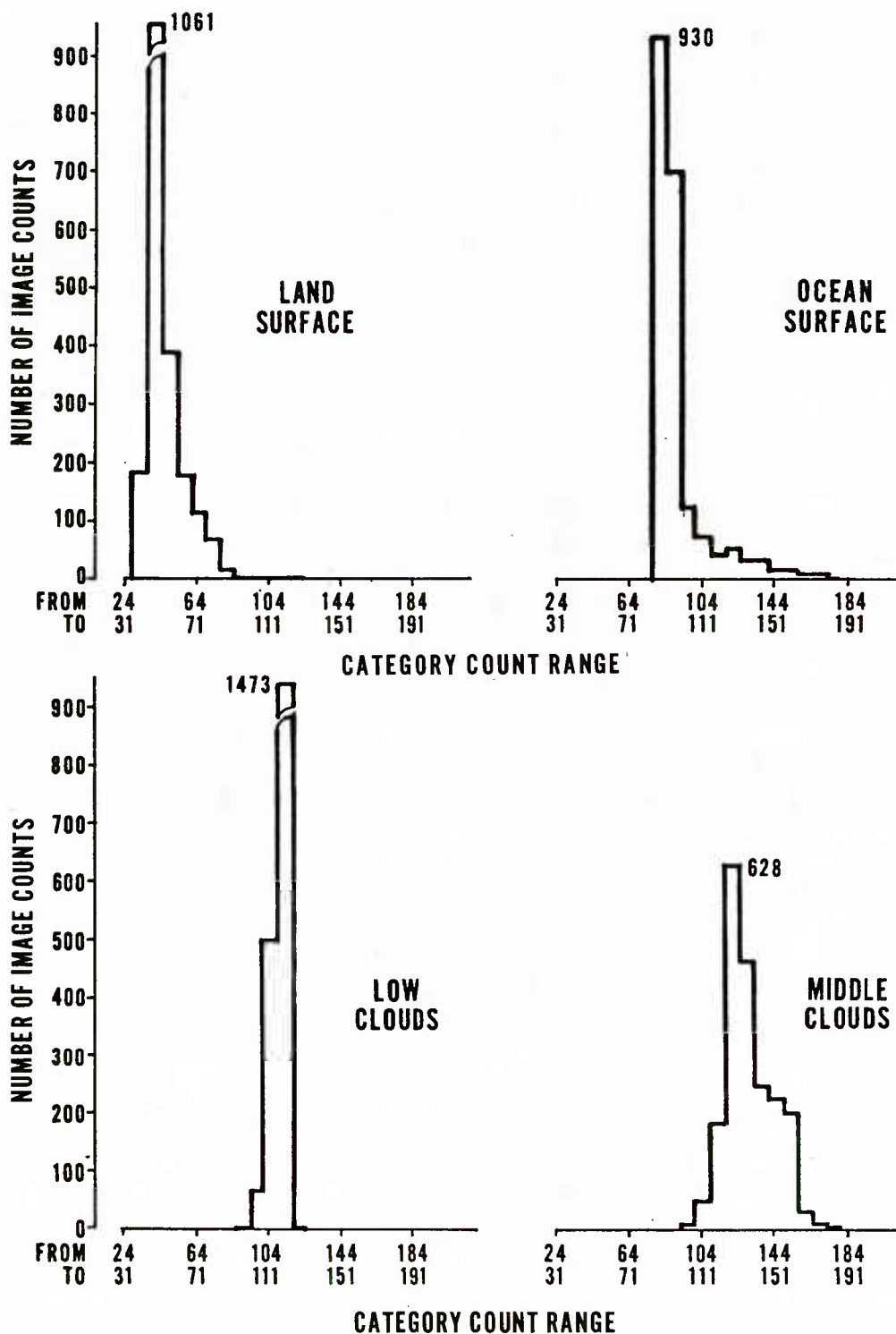


Figure 2a. Characteristic image count histograms for various surface/cloud situations. Plots show distribution of image counts for infrared subareas with mostly land surface, mostly ocean surface, low level clouds, and middle level clouds, respectively.

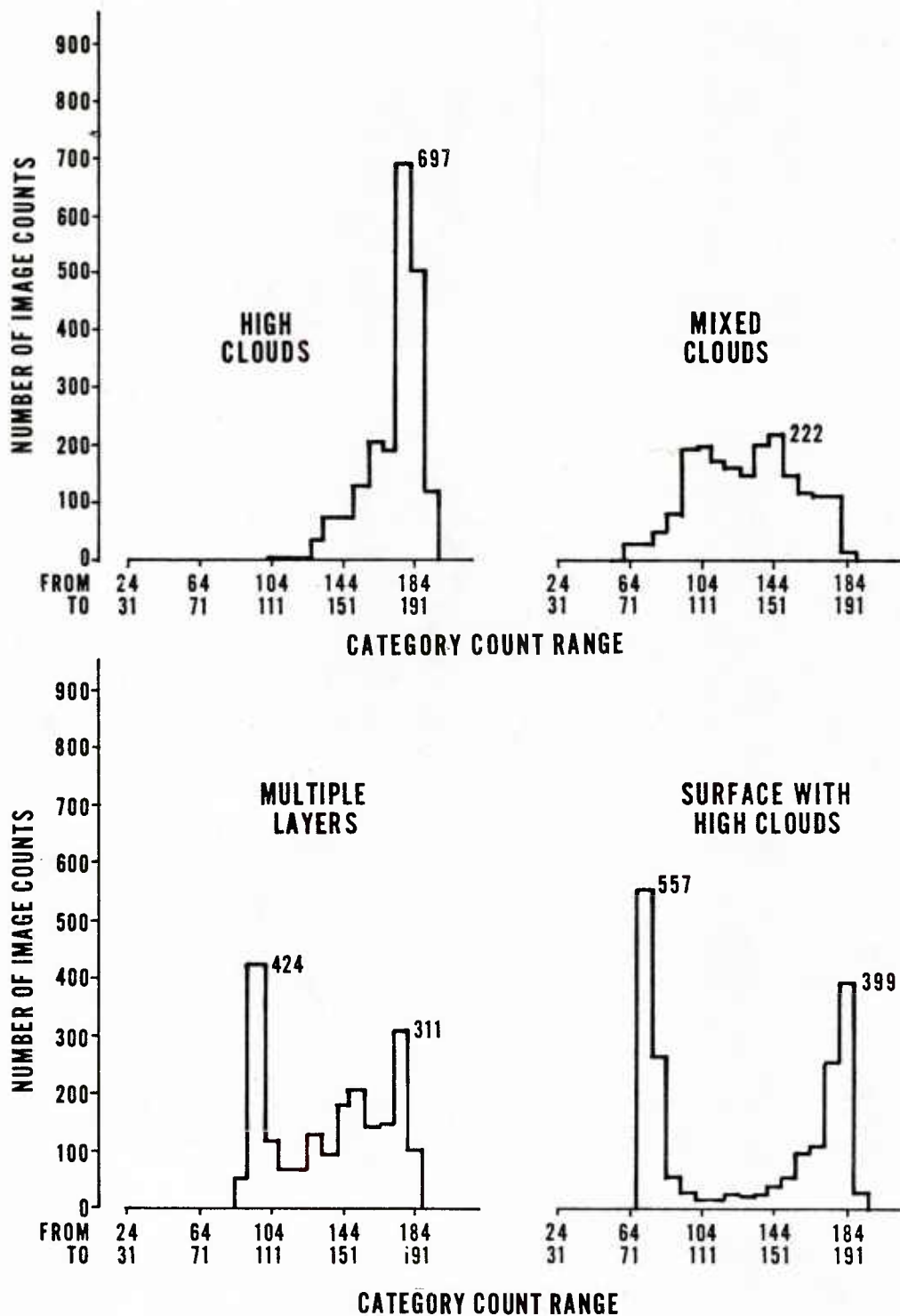
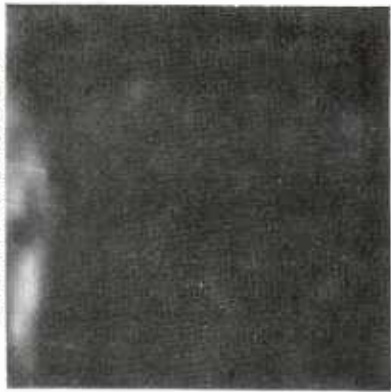


Figure 2b. Same as Figure 2a but for subareas with high level clouds, mixed level clouds, multiple layers of clouds, and surface and high clouds, respectively.

LAND SURFACE



OCEAN SURFACE



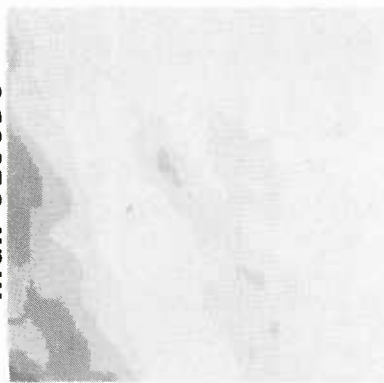
LOW CLOUDS



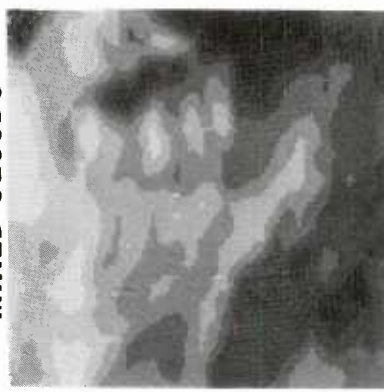
MIDDLE CLOUDS



HIGH CLOUDS



MIXED CLOUDS



MULTIPLE LAYERS



SURFACE/HIGH CLOUDS

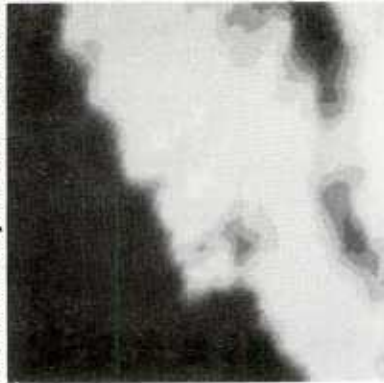


Figure 3. Infrared image subareas corresponding to histograms shown in Figure 2. Subareas are enlarged from 32 by 32 pixel image sections.

smoothing insures that categories with a zero value before smoothing remain zero after smoothing; the proper location of valley-to-valley slices is thus maintained. For an example of the effect of this smoothing, compare original histograms of high clouds and of multiple layers in Figure 2 with the smoothed distributions in Figure 4.

In subareas in which a majority of the area is cloud free and the maximum peak of the distribution is found at low count values, the slice includes only surface information. To prevent tracking land or ocean surfaces, the maximum distribution peak above a specified threshold is chosen. This threshold is a count value of 88 for infrared and 40 for visible data. If no peak other than one below the threshold occurs, no vector is computed. If another peak is identified such as in the "surface with high clouds" distribution of Figure 2, the slice is defined using the secondary peak.

Once the slice is defined, all values within the subarea of both images that are outside the range of the slice, are set to zero. Only clouds defined by the slice are tracked.

Details of the evolution of this slicing technique are included in Appendix A.

3.1.3 Edge and Pattern Enhancement

Because the XCOV method of computing cloud displacements is sensitive to the contrast within the satellite images, techniques for enhancing the contrast of the cloud pattern should increase the accuracy of resulting cloud motion vectors. One method of edge enhancement is to compute the standard deviation of each image element as compared to the eight adjacent elements, then to normalize the results, expanding to the entire 0 to 255 count range. Figure 5b shows an example of an image resulting from this standard deviation operation; Figure 5a is the original image for comparison.

Although this technique accurately enhances cloud edges, for use in this application the method is unsatisfactory. A decrease in contrast with a subsequent decrease in the accuracy of the XCOV results is produced. Patterns evident in cloud surfaces, as important to XCOV computation accuracy as the identification of edges, are eliminated.

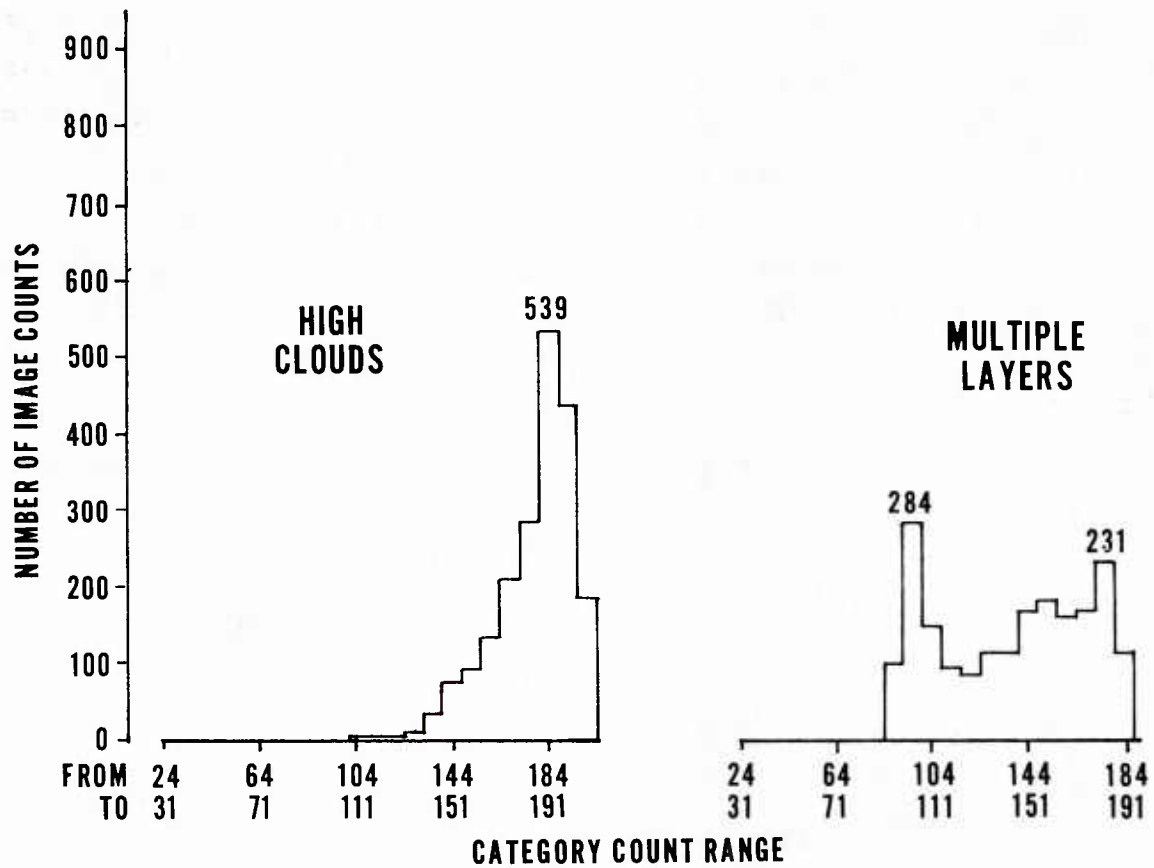


Figure 4. Same as Figure 2 but after applying smoothing algorithm. Subareas for high level clouds and multiple layers of clouds are shown.

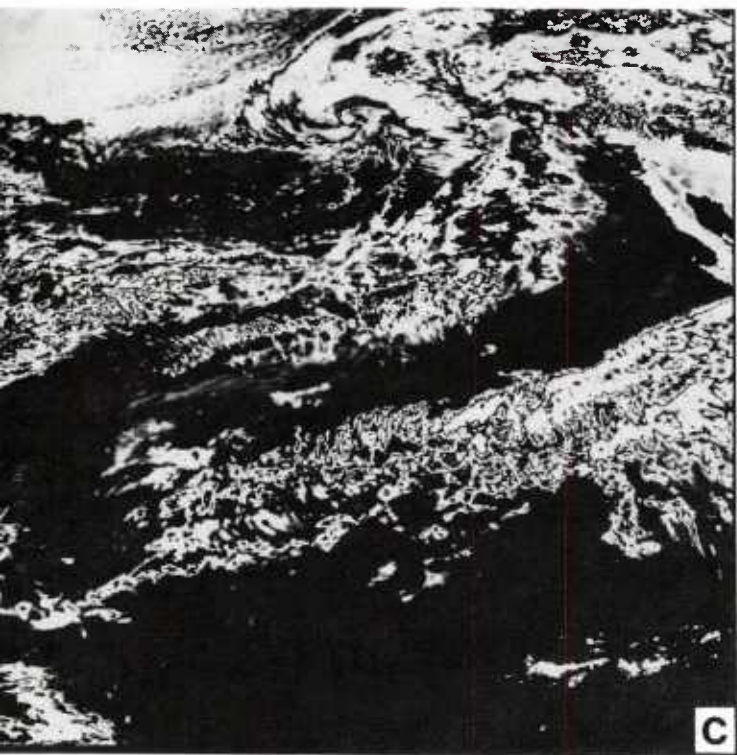
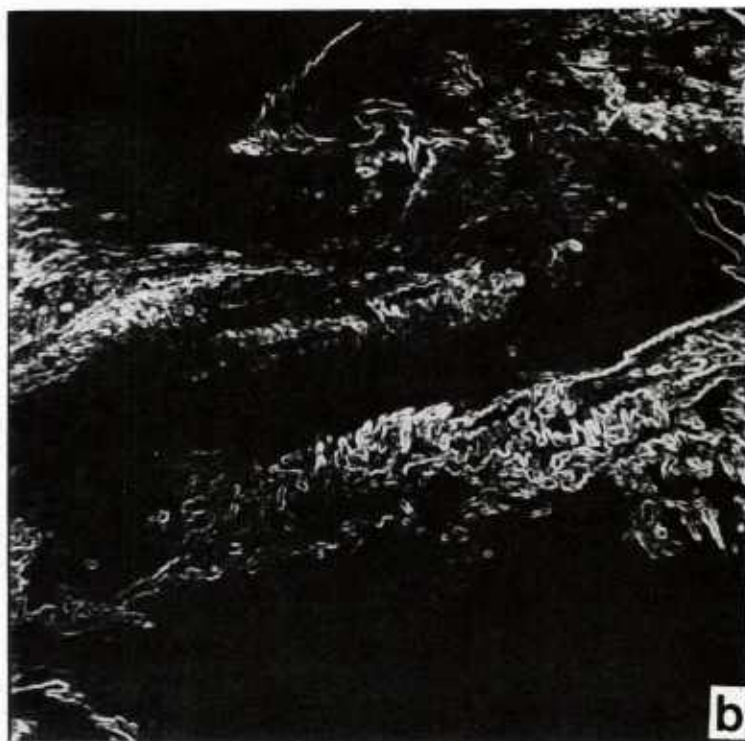
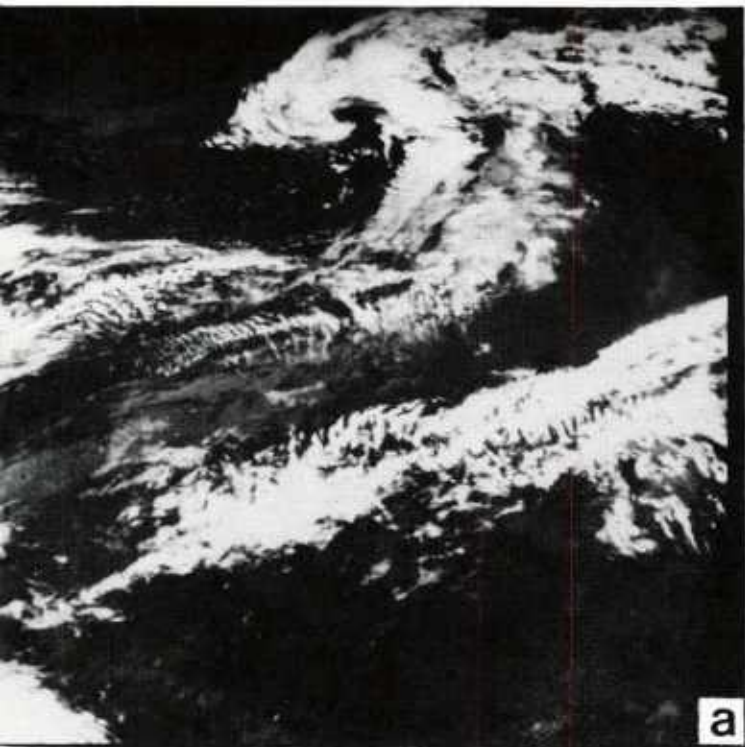


Figure 5. Results of infrared image edge and pattern enhancement. (a) Original unenhanced 8 km resolution infrared image. (b) Result of enhancement based on standard deviation. (c) Result of enhancement based on high order bit truncation.

A quick enhancement method which enhances both cloud surface patterns and edges was developed for SAWEGS: the two high order bits of the 8-bit infrared image counts are truncated. The effect of truncation upon the image counts is shown in Table 1; each set of 64 brightness values in the original range from 0 to 255 is assigned values from 0 to 63, thus producing sharply contrasting boundaries in the truncated image.

Table 1. Effect of high order bit truncation.

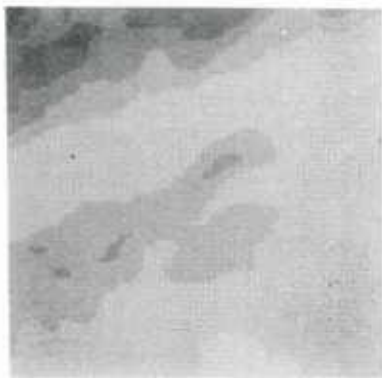
<u>Original Count Range</u>	<u>Count Range After Truncation</u>
0-63	0-63
64-127	0-63
128-191	0-63
192-255	0-63

Discarding the two highest order bits, bits which would appear to have the highest information content, may at first seem unorthodox and ill-advised. In essence, however, this technique simply sacrifices some count value information to enhance image pattern and edge information. This latter information is more important to the XCOV calculation. The effectiveness of truncation as an edge and surface enhancer is evident in the example in Figure 5c.

Truncation is applied only to infrared data. Visible satellite data is a measure of cloud thickness and the spatial density of cloud elements. Thus, truncation of visible data does not accentuate the roughness of cloud tops, as is true for infrared data, but instead enhances the thickness and size of the clouds. Due to this effect, tracking truncated visible data actually produces poorer results.

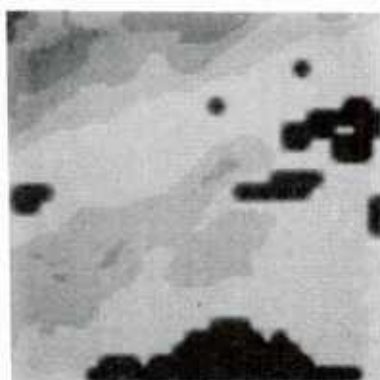
During the processing of one image subarea, the truncation technique is applied after slicing. Series of sample enlarged subareas for high clouds and for middle clouds (Figure 6) showing the original image, the sliced image, and the sliced/truncated image, illustrate the effects of these two operations.

HIGH CLOUDS

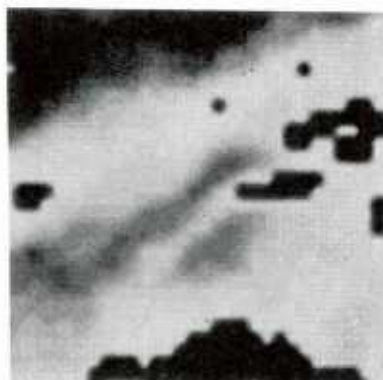
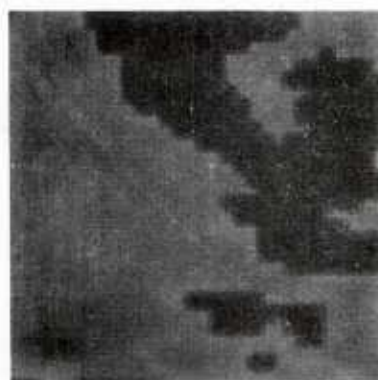


ORIGINAL IMAGE

MIDDLE CLOUDS



SLICED



TRUNCATED

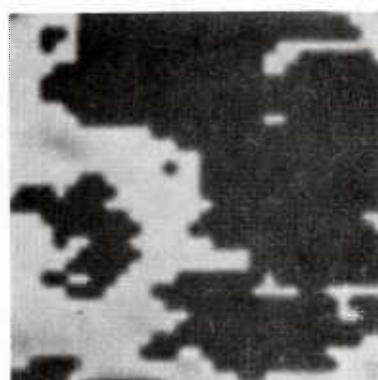


Figure 6. Examples of application of slicing and truncation. The original infrared subarea, the same area after slicing, and the same area after slicing and truncation are shown for a case of high level clouds and of middle level clouds.

3.2 CLOUD TRACKING

3.2.1 The XCOV Method

Following the preprocessing step, the XCOV matrix is computed from the two image subareas, one at each time. The XCOV computation becomes computationally feasible by use of the Fast Fourier Transform (FFT). The FFT redefines a function in the space domain, $f(x,y)$, with coordinates x,y into a function in the frequency domain, $F(u,v)$, with coordinates u,v . For an N by N set of discrete data, the two-dimensional FFT is defined by

$$F(u,v) = \frac{1}{N^2} \sum_{x=0}^{N-1} \sum_{y=0}^{N-1} f(x,y) \exp\left[-\frac{2\pi i}{N}(ux + vy)\right].$$

The inverse FFT, to convert a frequency domain function to the space domain, is given by

$$F^{-1}[F(u,v)] = f(x,y) = \frac{1}{N^2} \sum_{u=0}^{N-1} \sum_{v=0}^{N-1} F(u,v) \exp\left[\frac{2\pi i}{N}(ux + vy)\right].$$

Given arrays of brightness counts for two successive satellite images, $a(x,y)$ and $b(x,y)$, the XCOV is

$$C(x,y) = F^{-1}[A^*(u,v) \cdot B(u,v)],$$

where $F^{-1}[\]$ indicates the inverse FFT of the enclosed quantity, A and B are forward FFT of a and b , and A^* is the complex conjugate of A . The position of the maximum value of the XCOV matrix within the matrix indicates the relative displacement from image a to image b . A set of geostationary satellite images, divided into subareas of N by N image elements, produces a vector for each subarea within which clouds exist.

3.2.2 XCOV Matrix Origin Determination

The matrix resulting from the XCOV computation represents four possible displacements, each of which is realized by assuming that the XCOV maximum is in one of the four possible quadrants of a super-matrix. Figure 7 depicts these possibilities. Assuming the matrix maximum is in the lower right quadrant, the displacement vector is vector OA (O is the origin of the super-matrix).

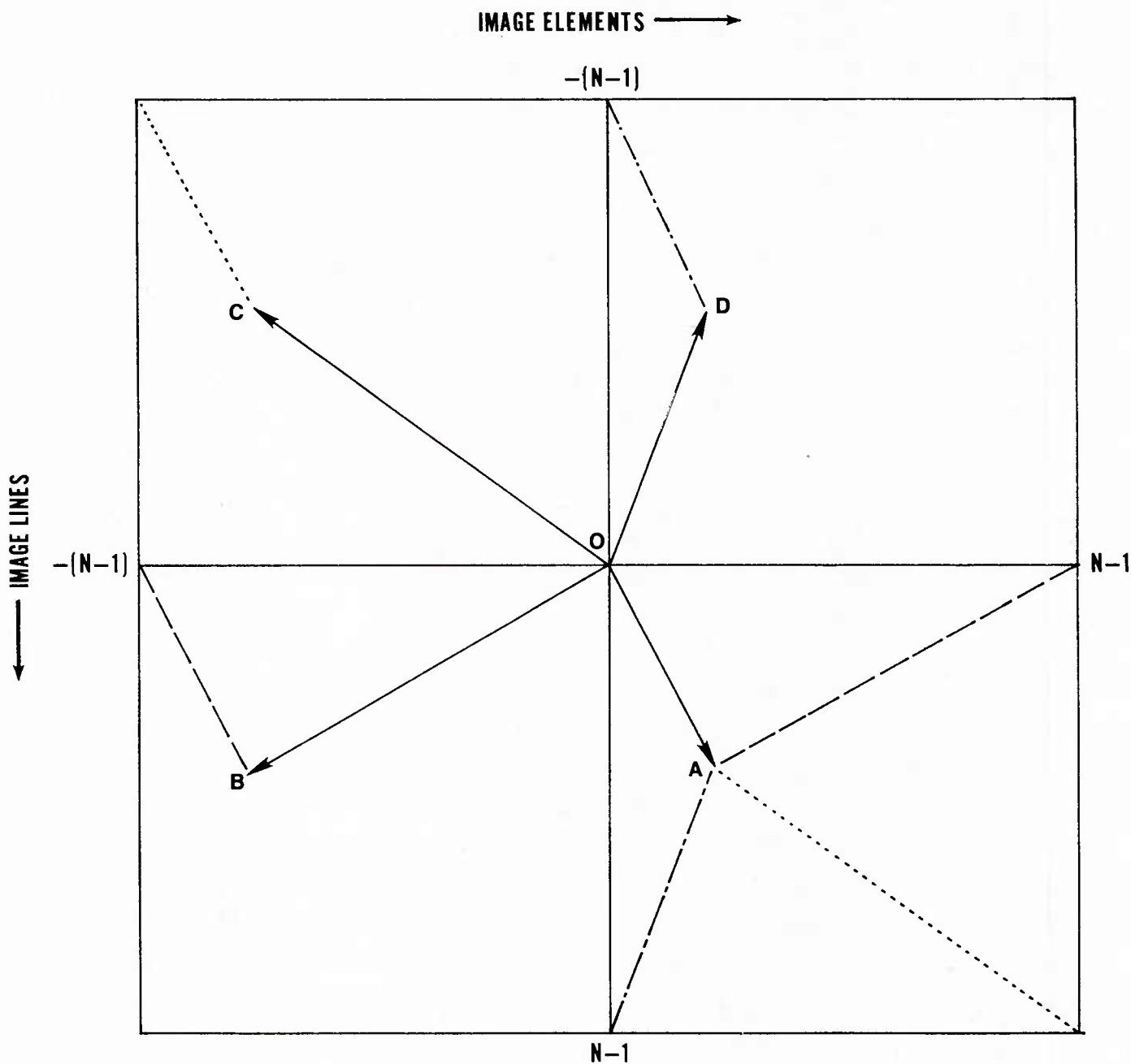


Figure 7. Depiction of four possible origins in the cross-covariance matrix. Each quadrant represents the identical matrix resulting from a cross-covariance computation. Solid vectors depict four possible vectors; dotted/dashed lines show cyclic wraparound produced by FFT's periodicity.

However, because of the FFT's cyclic nature (shown by the dashed/dotted lines in the figure) the maximum may represent points B, C, or D in the other quadrants giving displacement vectors of OB, OC, OD, respectively. Thus, all four points are actually the same points in the XCOV matrix, but the actual displacement may be interpreted from the matrix using any of four points as the matrix origin. The result is a choice of four possible displacements.

For example, if the maximum XCOV value is located at matrix location 14,10 using 32x32 image element subareas, the possible displacements are (13,9), (13,-23), (-18,9), and (-18,-23). The question is, "Which origin gives the correct displacement?" In an effort to answer this question, a number of methods were tested; these methods are discussed in Appendix B.

A simple method of origin determination was ultimately included in SAWEGS. If a correct balance of image horizontal and temporal resolution and of subarea size are used for tracking, identifying the XCOV matrix origin closest to the maximum XCOV value as the correct origin proves to be the best method. For example, with 8 km infrared images 30 minutes apart and a subarea size of 32x32 image elements, matrix origins for cloud motions of up to between 70 m/s and 100 m/s are identified correctly. This speed, in the range of the maximum speed of an intense tropical storm, allows correct origin determination for nearly all cloud motions. For 4 km images, the 35 m/s to 50 m/s maximum speed is more likely to cause some problems, but is still acceptable in many cases.

Since experimentation showed that in most cases of an incorrect vector due to an incorrect origin selection, adjacent vectors were correct, the quality control should delete the incorrect winds. To provide an ample number of correct vectors for quality control in close proximity to potentially incorrect vectors, four passes through the data are made. Each pass shifts the line or element a distance equal to one-half the subarea size, thus creating overlapping subareas.

3.2.3 No-Tracking Tests

During tracking, conditions which are known to produce incorrect vectors exist in some subareas. These conditions include subareas in which no clouds are evident or in which a subarea does not contain information necessary for accurate use of the XCOV operation. The cloud tracking system must identify these conditions and bypass the tracking procedure when they exist.

No-cloud conditions are eliminated by testing for distribution peaks of counts which fall below the threshold values set as part of the slicing operation. If no peaks exist above the threshold level, a no-cloud condition is assumed and no tracking is applied for that subarea.

Several conditions produce erroneous vectors because of the nature of the XCOV algorithm. SAWEGS eliminates tracking in subareas containing low contrast image fields, uniform histogram distributions, or too few non-zero count values. A subarea is bypassed for tracking if the difference between the maximum and minimum count values in either image is less than four counts.

The XCOV algorithm has a similar problem when few non-zero count values remain within a subarea after slicing. This condition often occurs, especially when the majority of count values are below the background threshold and slicing is applied with limits set using a small secondary peak of the count distribution. To prevent problems attributed to this condition, tracking is bypassed if less than 100 of the 2048 possible image elements in the subarea images are non-zero.

Uniform distributions of counts -- fields with no dominant count value -- may also cause problems. If a subarea's count histogram distribution has many extrema, none of which is dominant, slicing is ineffective. This condition is detected by testing the number of extrema in the distribution. If the number of extrema exceeds ten, no tracking is done.

3.3 HEIGHT ASSIGNMENT

Assignment of heights to the resultant displacement vector assumes that the average infrared count value in the subarea after slicing estimates the value of cloud elements moving with the computed displacement vector. This count value is converted to a temperature using the set of conversions

if $B \leq 178$, $T = 331.-B/2$,

if $B > 178$, $T = 420.-B$,

where B is count and T is the resulting temperature. A representation of this conversion curve is shown in Figure 8.

Temperature is converted to height by utilizing the Navy operational upper air temperature analysis fields generated at the Fleet Numerical Oceanography Center. A profile of temperatures at standard analysis levels and at the analysis grid point nearest the center of the tracking subarea is constructed from the analysis fields. A pressure height corresponding to the temperature derived from the count value is linearly interpolated in log of pressure from the analysis profile. This height is assigned to the cloud motion vector. At the present time, no corrections for emissivity or for cloud thickness are included.

3.4 EARTH LOCATION AND WIND VECTOR COMPUTATION

At the conclusion of tracking cloud movement in a particular subarea, resulting vector endpoints specify the displacement in image coordinates. Earth location and vector computation are required to convert the displacement to a wind vector at a specific latitude and longitude.

Earth location is accomplished using the National Environmental Satellite Service's (NESS) navigation software (Westinghouse Electric Corporation, 1977). NESS-derived Chebychev polynomial coefficients are transmitted to the satellite as part of the "stretched-mode" Infrared Orbit and Altitude Documentation data record, and are subsequently retrieved at NEPRF, along with the image data, using the GOES Acquisition and Data Handling System

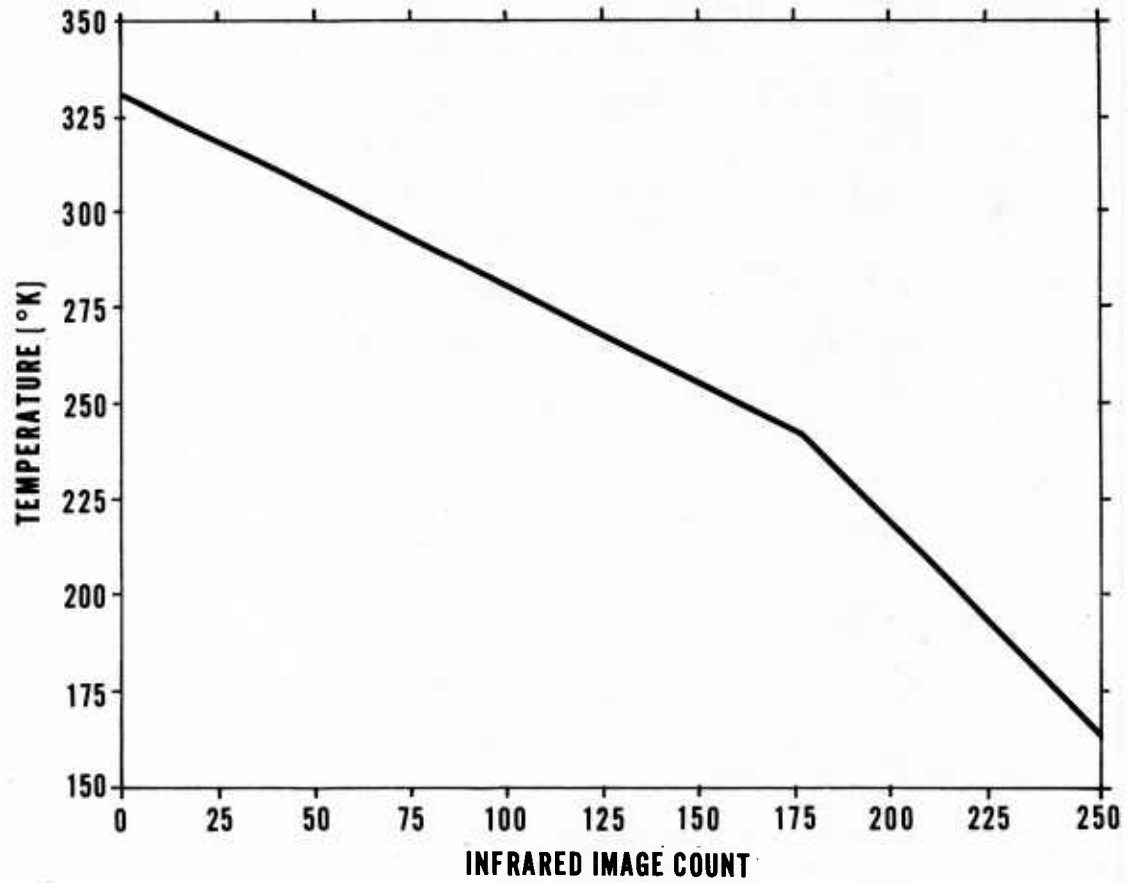


Figure 8. Conversion of infrared image count to temperature for SAWEGS height assignment.

(Nagle and Lee, 1979). Subroutines supplied by NESS then utilize the information in this data record to transform any set of image coordinates to earth coordinates.

Once the vector endpoints representing the cloud motion displacement are earth-located, a wind speed and direction is computed from the arc distance between these points and the time difference between images.

The XCOV-deduced cloud motion vector represents the displacement of all motions in one image subarea relative to all motions in the same subarea in a subsequent image; therefore, no one cloud element is actually tracked. Thus, no one geographical location, such as an average position of a cloud feature in the two images, is identified. At the present time, a vector is located at the center of the subarea.

3.5 QUALITY CONTROL

Flagging incorrect or inconsistent vectors produced by SAWEGS is accomplished by an objective quality control (QC) system. The current QC configuration includes four passes through a basic two-step procedure. The Analysis step averages the observations to produce a smooth wind field. The Discard step compares the observations to the analyzed wind field and flags inconsistent vectors. Subsequent passes refine the quality of the observations.

A unique characteristic of the wind observations, a result of locating each vector at the center of the subarea, is that observations are regularly spaced. This fact allows the analysis grid and the observations to be colocated and simplifies the search for observations near an analysis field grid point.

The Analysis step computes separate weighted averages of the observations' u- and v- components within a given height range. The averages,

$$u_A = \frac{\sum_{n=1}^N u_n w_n}{\sum_{n=1}^N w_n} \text{ and } v_A = \frac{\sum_{n=1}^N v_n w_n}{\sum_{n=1}^N w_n} ,$$

where u_n , v_n are the observation wind components and w_n are the corresponding weights, are computed for diamond-shaped frames surrounding the analysis grid point. Observations in frames one and two grid lengths from the grid point are averaged; if fewer than five observations are available in these two frames, up to two more increasingly larger frames are averaged until five or more observations are included (Figure 9). The weighting factor for each observation is the inverse of the distance from the analysis point.

The analysis step for subsequent passes through the observation averages only those observations not flagged by the previous Discard step.

Within the Discard step a discard factor is computed for each observation in comparison with the colocated analysis grid point value. This factor D is given by

$$D = \frac{50[(u_o - u_A)^2 + (v_o - v_A)^2]^{1/2}}{1/2[(u_o^2 + v_o^2)^{1/2} + (u_A^2 + v_A^2)^{1/2}]}$$

where u_o , v_o are observation wind components and u_A , v_A are components of the analysis wind. The multiplier 50 increases the D value to produce values in the range from 0 to 100. In physical terms the discard factor represents a ratio of the magnitude of the wind difference between the observation and the analysis to the average of the magnitude of the observation wind and of the analysis wind.

If the discard factor for an observation is greater than a specified tolerance, the observation is flagged. All observations, including those flagged in a previous pass, are quality checked on each pass; only those observations flagged on the final pass are actually discarded.

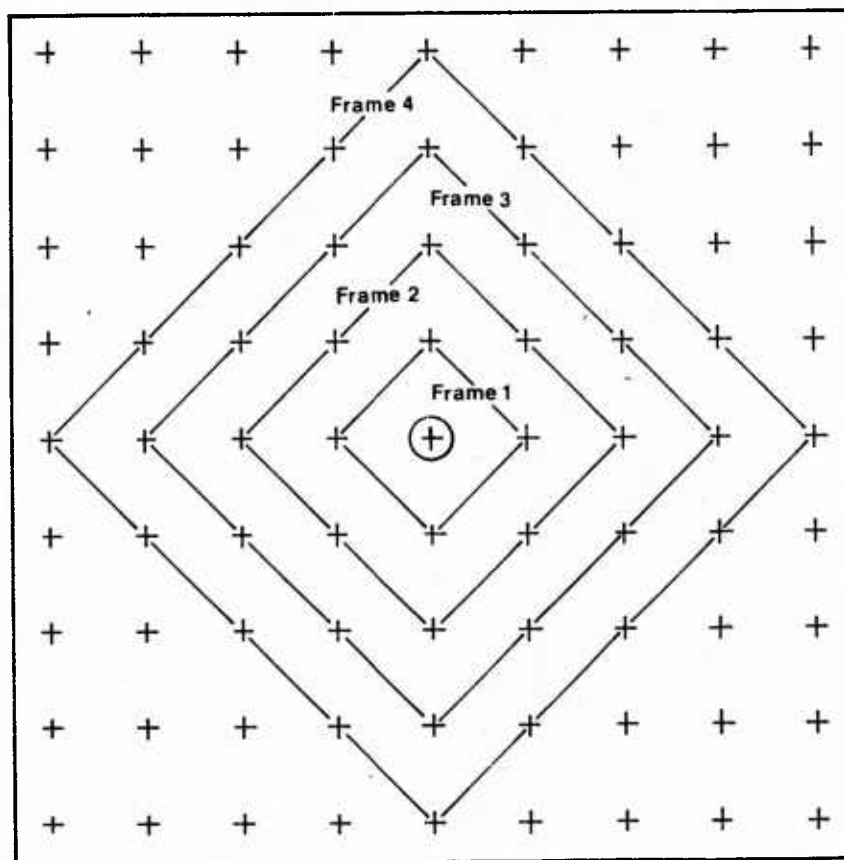


Figure 9. Quality control analysis frames. Beginning with the frame of four closest grid locations, increasingly larger frames of observations are averaged until five or more observations are included. If five observations are not found in four frames (40 grid locations), these observations found in the four frames are averaged.

4. APPLICATION RESULTS

This section presents results of the application of SAWEGS to three different data sets. Because the quality control program was not complete at the time these data sets were processed, these examples are not quality controlled.

4.1 INFRARED

Infrared GOES-WEST satellite images for 26 March 1979, 2115 and 2145 GMT, have been used extensively in testing during the development of the SAWEGS. The data were retrieved at 8 km resolution; cloud motions were tracked using a 32 by 32 subarea size resulting in a 128 km resolution mesh of wind vectors. The area selected for tracking shows a low pressure system with associated fronts located off the west coast of the United States, and a well-defined subtropical jet moving to the northeast and located just south of the Baja Peninsula (Figure 10).

Vectors computed for this case were plotted at three levels and overlayed on the image (Figure 11). These levels -- 1100 to 800 mb, 800 to 500 mb, and above 500 mb -- approximate winds for low, middle, and high clouds, respectively.

The low level vectors for this case are characteristic of the good quality of SAWEGS-produced cloud motion vectors. Low level clouds to the northwest of the low pressure vortex detect the cyclonic flow as do the winds south of the low and behind the front. An examination of satellite image loops confirm that these vectors represent motions of the clouds and not of the various meteorological systems.

Despite the high percentage of reasonable vectors, a few of the vectors are obviously incorrect or are inconsistent with neighboring vectors. Along the coast, vectors of very different speeds and directions are evident; a combination of stationary low level coastal fog below and patches of thin cirrus above result in vectors with a combination of motions and with incorrect height assignments.

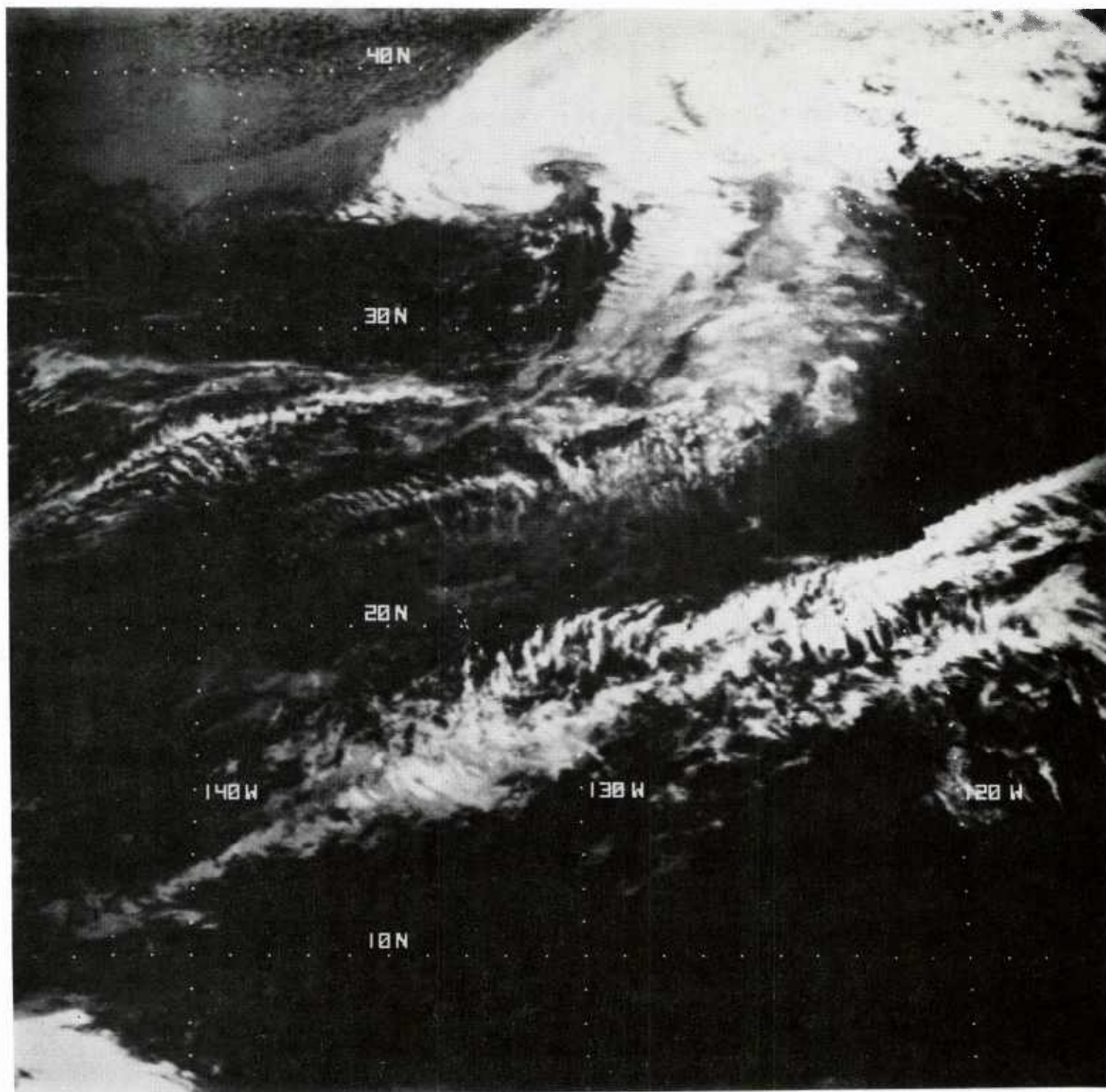


Figure 10. Infrared GOES-West image for 26 March 1979, 2115 GMT; resolution is 8 km.

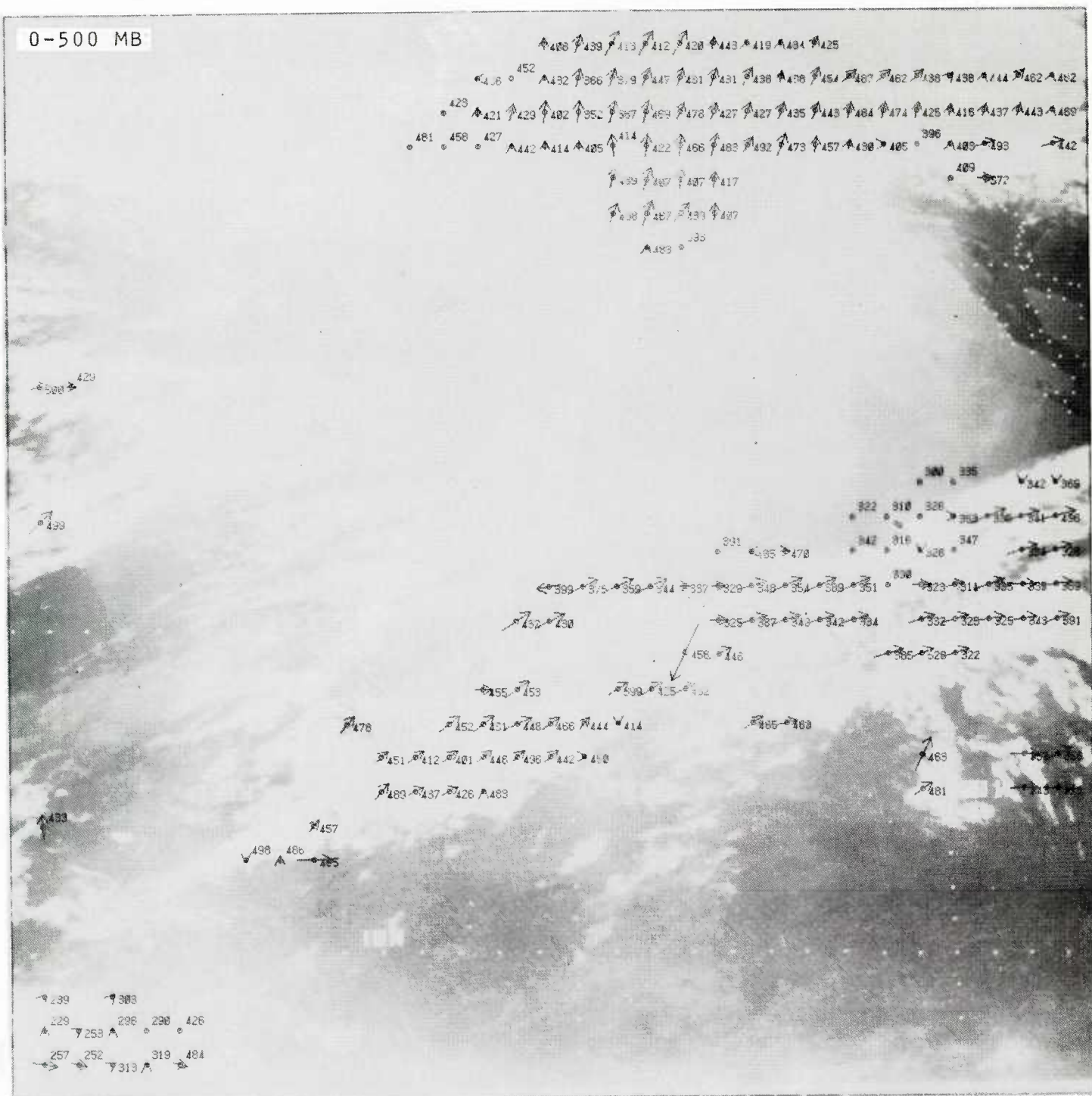
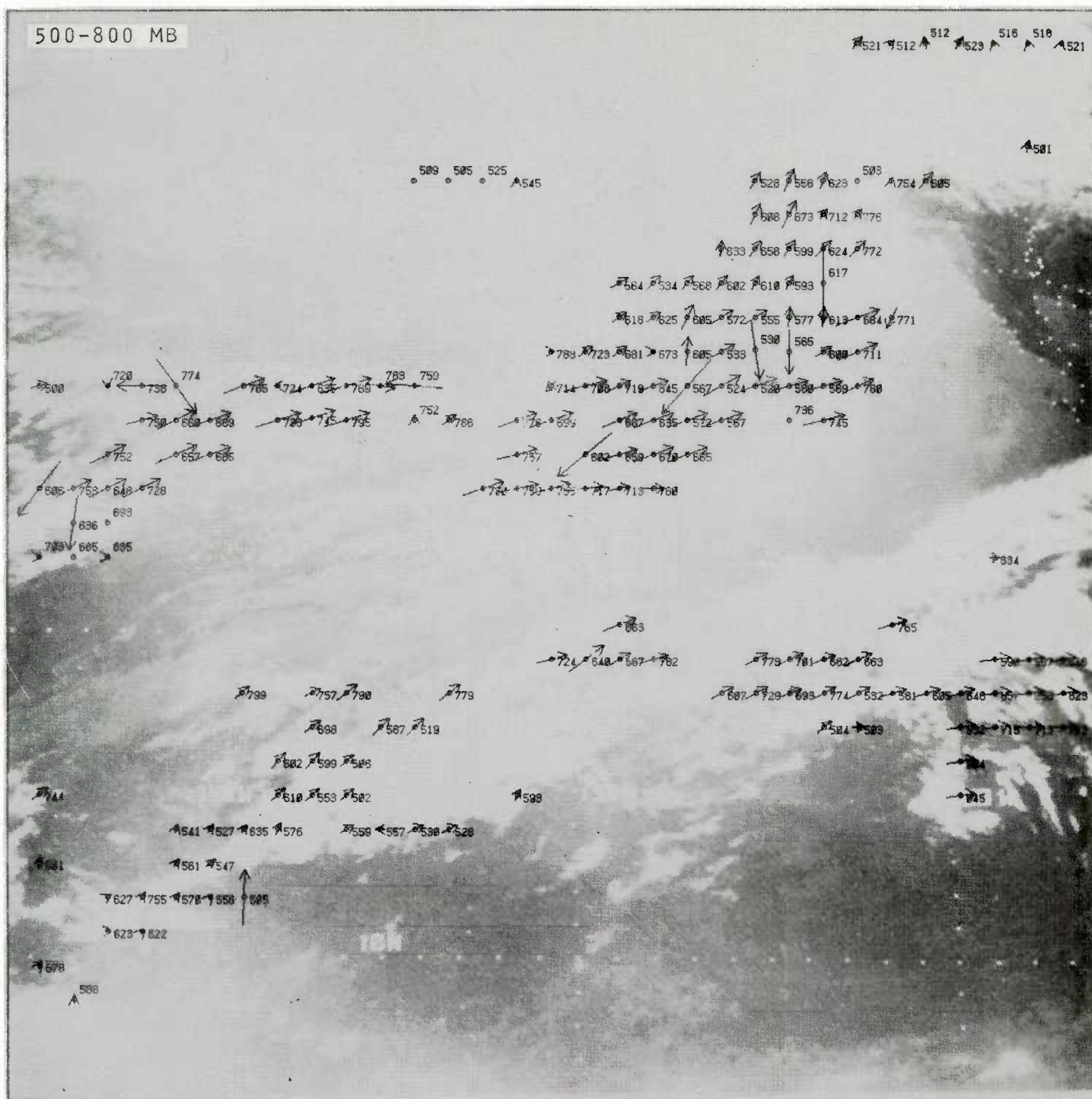


Figure 11a. SAWEGS vectors for upper levels produced by tracking 26 March 1979, 2115/2145 GMT infrared image pair. A 32 by 32 subarea size was used with a 16 pixel overlap of subareas. Vector length is proportional to wind speed; numerals with each observation indicate height in millibars. Quality control has not been applied.

512 516 518
521 512 523 521



30

800-1100 MB

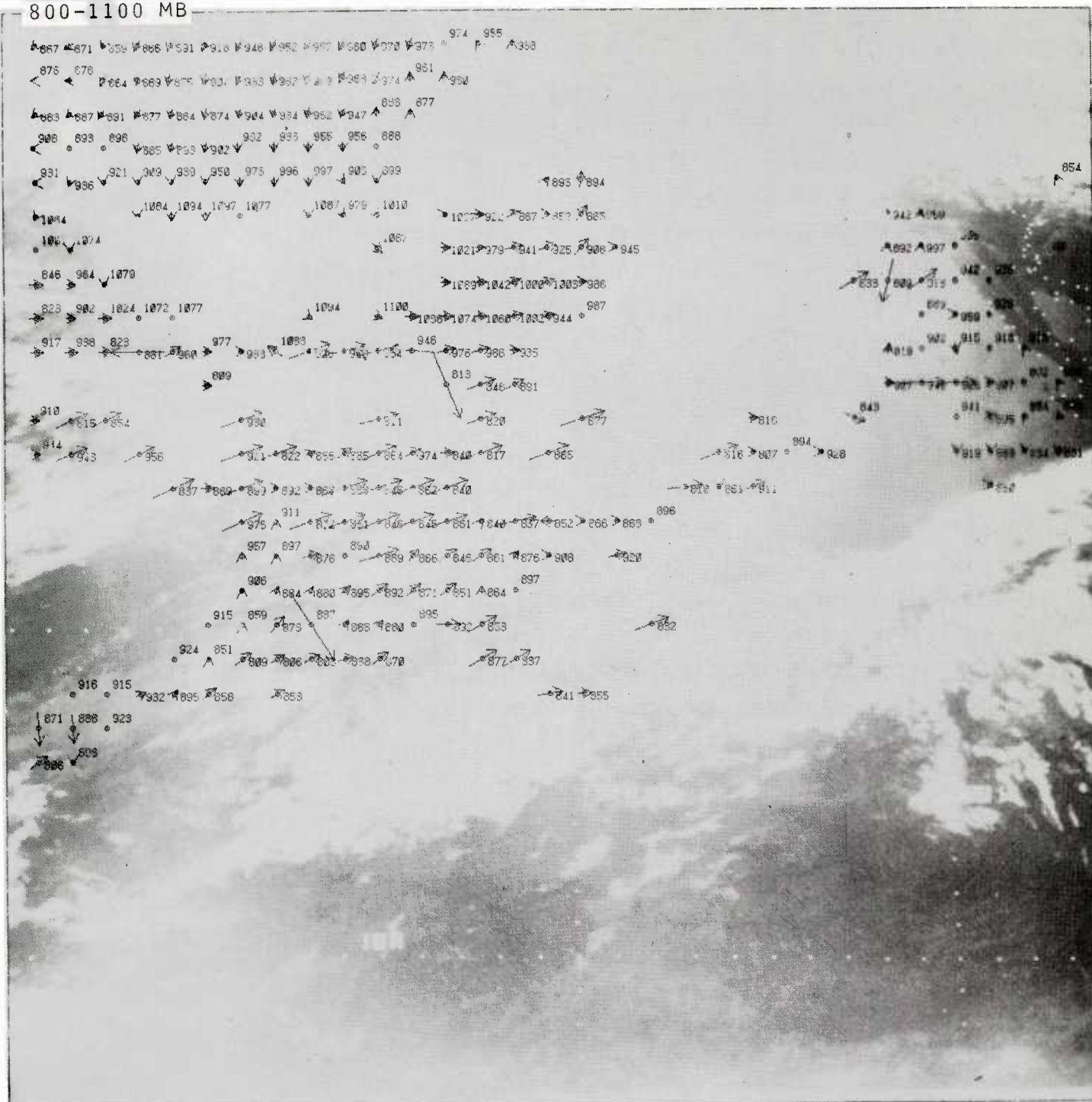


Figure 11c. Same as 11a and b, but for lower levels.

Other vectors appear to be associated with the jet, but are assigned to low levels. Inspection of image loops of subareas after slicing and of the associated histogram suggest a reason for this paradox. The subareas producing these vectors contain large areas of ocean surface, in some cases covered by a thin cirrus layer, with patches of highly reflective clouds associated with the jet. Unfortunately the histogram peaks just above the surface threshold value and the slicing limits are set for the low count values. Once slicing is applied, areas of high clouds associated with the jet are given zero count value. These zeroed areas, however, produce a high correlation between images. So, although the displacement represents the cloud movement, the level assignment is at a low level.

Overall results are similar for the middle and upper levels. A greater number of inconsistent motions are evident in the middle level vector field, most likely due to the attempts of the slicing algorithm to discern middle level motions from motions at upper and at lower levels.

Upper level divergence in the northeast quadrant of the low pressure system is evident in the upper level wind field as is an increasingly eastward component in the jet stream cloud motion vectors as the jet nears the coast.

Calm winds appear in areas they should not. Upper level calm winds near the center of the low result from the negating effect of mixed cloud motions associated with the cyclonic system. Calm winds along the northern edge of the jet result from the dominating influence of low clouds and of the ocean surface upon the cross-covariance algorithm in these regions. This problem is related to that of low level heights assigned to upper level motions discussed previously.

4.2 VISIBLE

Although future plans include coupling infrared and visible data for tracking, the current version of SAWEGS processes each channel separately. This section presents an example of tracking using visible data.

GOES-WEST images for 30 October 1979, 2015 and 2045 GMT, with 8 km resolution and a 32 by 32 subarea size were processed. The area selected shows a weak low pressure center off the Washington coast and a large high pressure system south of the low with associated stratocumulus cloud structure (Figure 12).

Because visible and infrared data are used separately, no infrared data is available for height assignment of vectors derived from visible data. Also, as explained previously, no truncation of high order bits is applied to visible data.

The quality of resulting vectors for this case is again good. The flow depicted by vectors extracted in the stratocumulus region correspond to motions depicted in image loops as do most of the vectors around the low and the vectors associated with another low off the northwest corner of the image area. A series of north-northeast-moving cirrus cloud streaks at 20°N and 135°W, barely evident in the single image, were successfully tracked despite the opposing low level flow. Vectors are shown in Figure 13.

As is immediately evident, the system identifies vectors in clear regions, including calm winds. Over the ocean this problem can be eliminated by increasing the surface brightness threshold value used in the slicing algorithm. However, because the land surface brightness values in the visible are often quite high, elimination of tracking in these areas must be accomplished by using the infrared data to detect the land surface influence. Note that, although incorrect, the zero vectors resulting from tracking land surfaces confirm the effectiveness of the SAWEGS earth location program.

4.3 TROPICAL CYCLONE

Because of the cirrus clouds, rapid convection, and high speeds characteristic of tropical cyclones, extraction of cloud motion vectors around these systems has always been a challenge. To test the system on a difficult data set, the SAWEGS was applied to a tropical storm case. Infrared images of 4 km resolution for East Pacific Hurricane Delores, 19 July 1979, 2015 and 2045 GMT, were processed using a 64 by 64 subarea size. The image for 2015 GMT is shown in Figure 14.

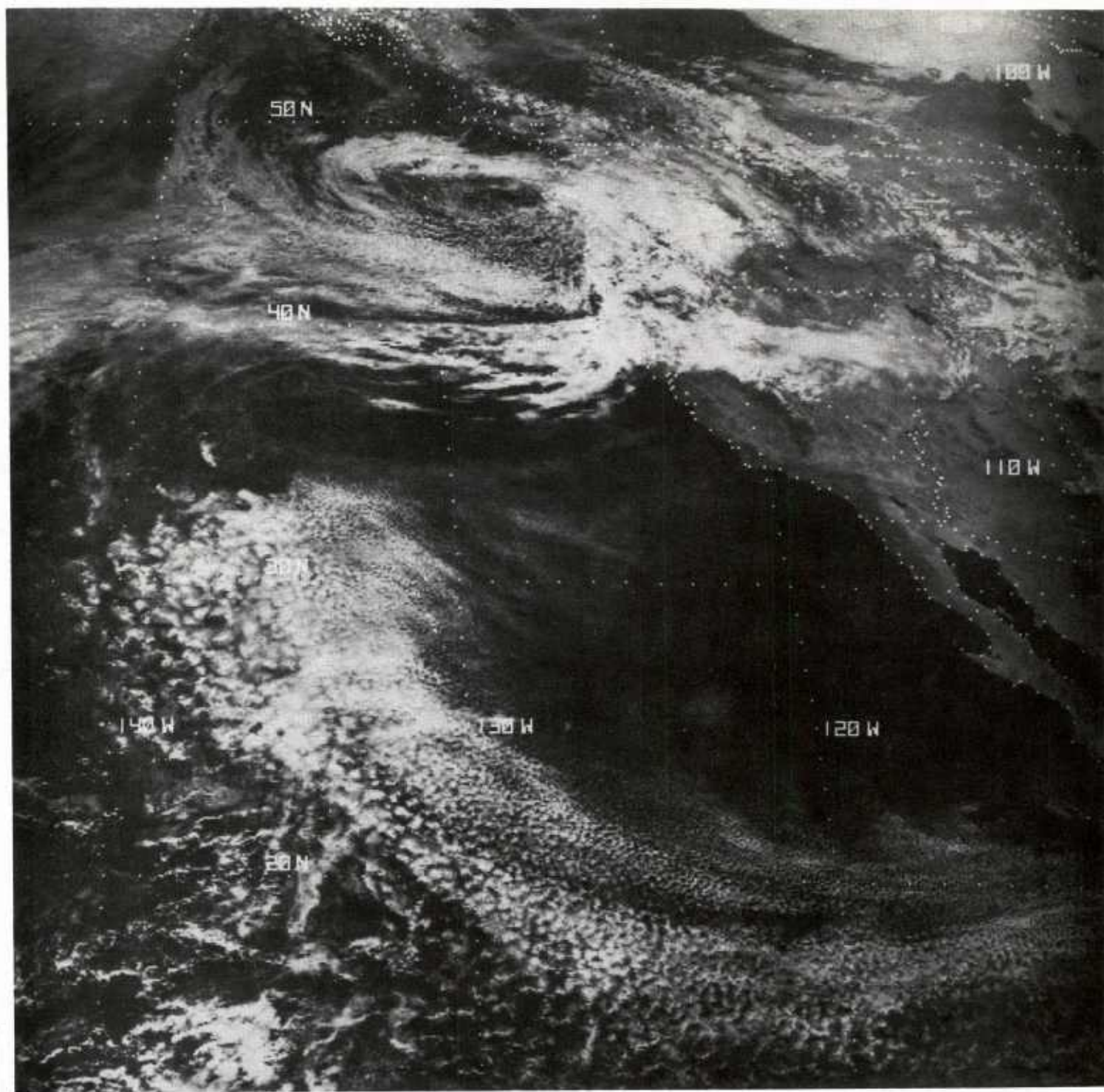


Figure 12. Visible GOES-West image for 30 October 1979, 2015 GMT; resolution is 8 km.

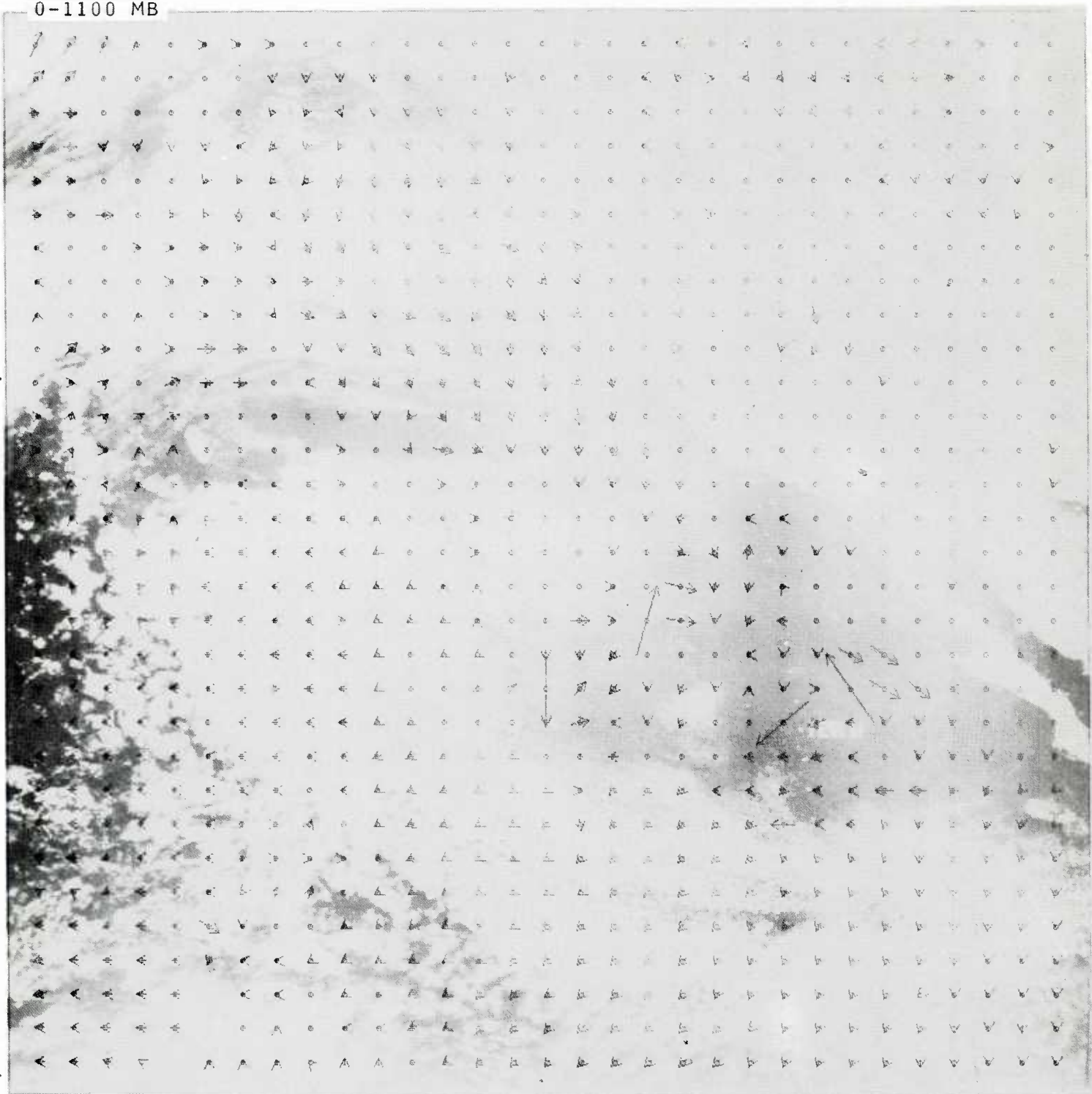


Figure 13. SAWEGS vectors produced by tracking 30 October 1979, 2015/2045 GMT visible image pair. A 32 by 32 subarea size was used with a 16 pixel overlap of subareas. Vector length is proportional to wind speed. Quality control has not been applied. Heights are not computed when tracking visible channel data.

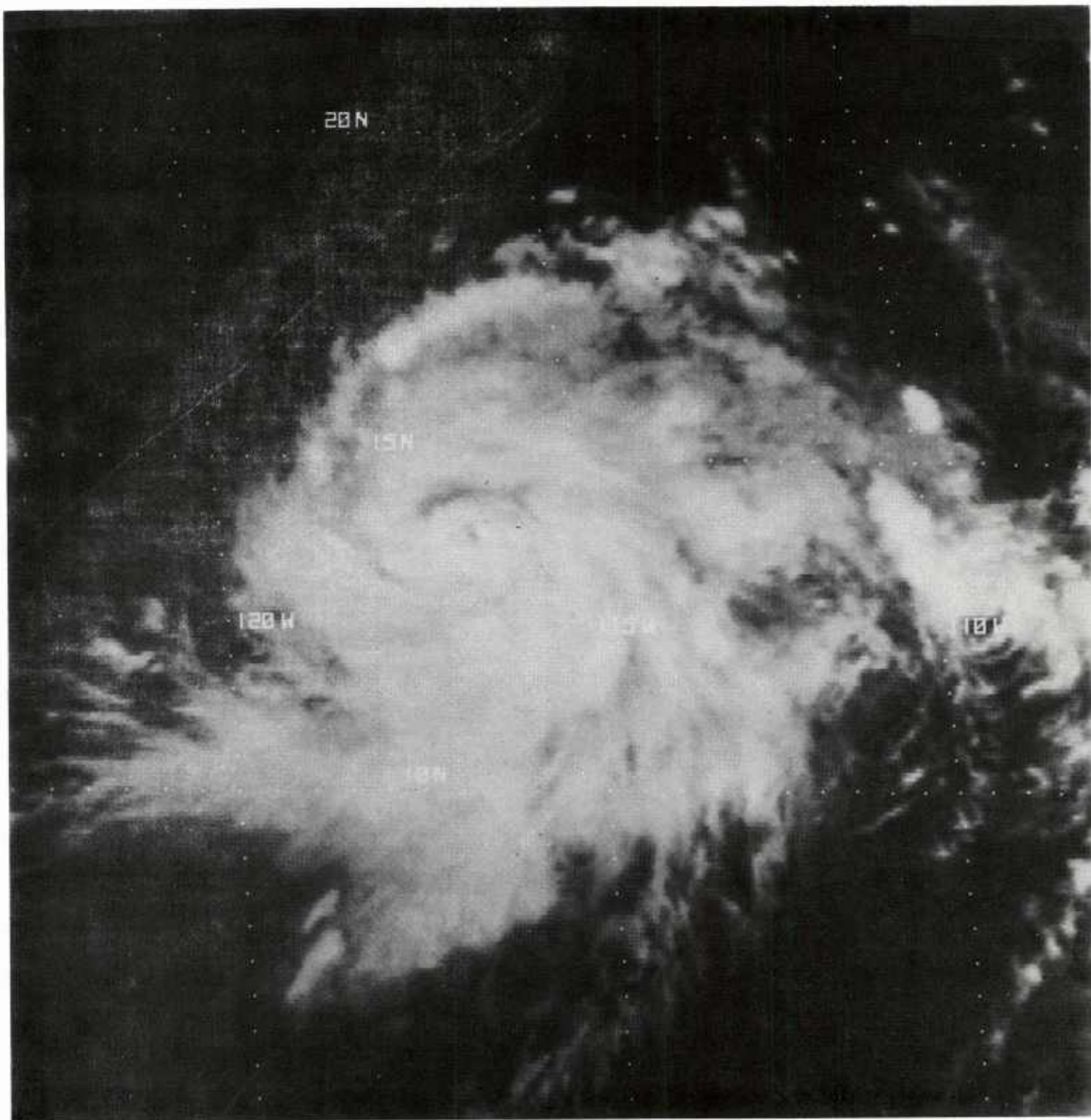


Figure 14. Infrared GOES-West image of hurricane Delores,
19 July 1979, 2015 GMT; resolution is 4 km.

The resulting vectors are encouragingly good. Cyclonic motion around the eye, and outflow bands to the west, southwest, and east are well represented. The northwest movement of the hurricane may have influenced the directions of vectors just north of the eye. Other vectors are obviously in error, but should be eliminated by application of the quality control program. Vectors are shown in Figure 15.

4.4 EFFECT OF SUBAREA SIZE

Because of the wind speed limit for effective XCOV matrix origin determination, and because of the direct inverse relationship which exists between subarea size and image resolution, maintaining a proper balance among the image resolution, the time interval between images, and the subarea size is very important. In this section examples of changing the subarea size are presented.

A subarea size smaller than the optimal size for a given image resolution and time interval will result in degradation of the vector quality. The Hurricane Delores case shown previously was tracked using a 64 by 64 element subarea size. Results of the same data tracked with 32 by 32 element subareas reveal a large number of contradicting, confusing motions. The upper level vectors for this case are shown in Figure 16; they should be compared with the case for the larger subarea size in Figure 15.

If, on the other hand, subarea size is increased, an even better-quality set of vectors results. The infrared example for 26 March 1979 tracked 30 minute, 8 km resolution images with 32 by 32 element subareas (Figure 11). An identical experiment for the same data but with 64 by 64 element subareas and with a larger overlap of subareas was performed for comparison; the resulting vectors are shown in Figure 17.

The larger subarea size implies fewer subareas and thus would produce approximately one-quarter as many vectors. But with a larger subarea overlap resulting in 16 passes through the data, the number of vectors remains nearly the same as the 32 by 32 case. However, the large subarea size allows more information to influence the displacements produced by the XCOV operation, producing a smoother, apparently more accurate set of vectors.

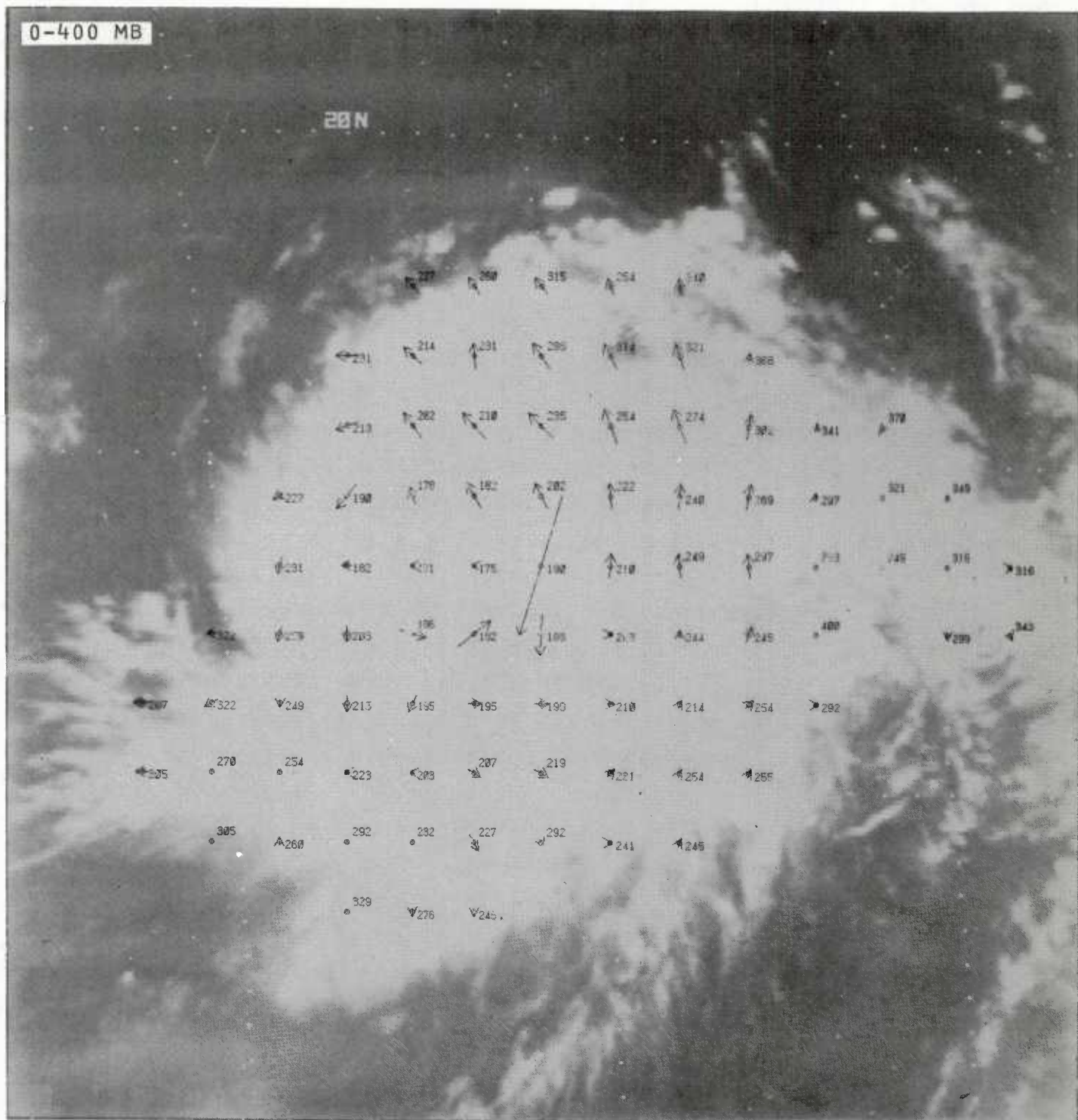


Figure 15a. SAWEGS vectors for upper levels produced by tracking 19 July 1979, 2015/2045 GMT infrared image pair. A 64 by 64 subarea size was used with a 32 pixel overlap of subareas. Vector length is proportional to wind speed; numerals with each observation indicate height in millibars. Quality control has not been applied.



Figure 15b. Same as 15a, but for middle levels.

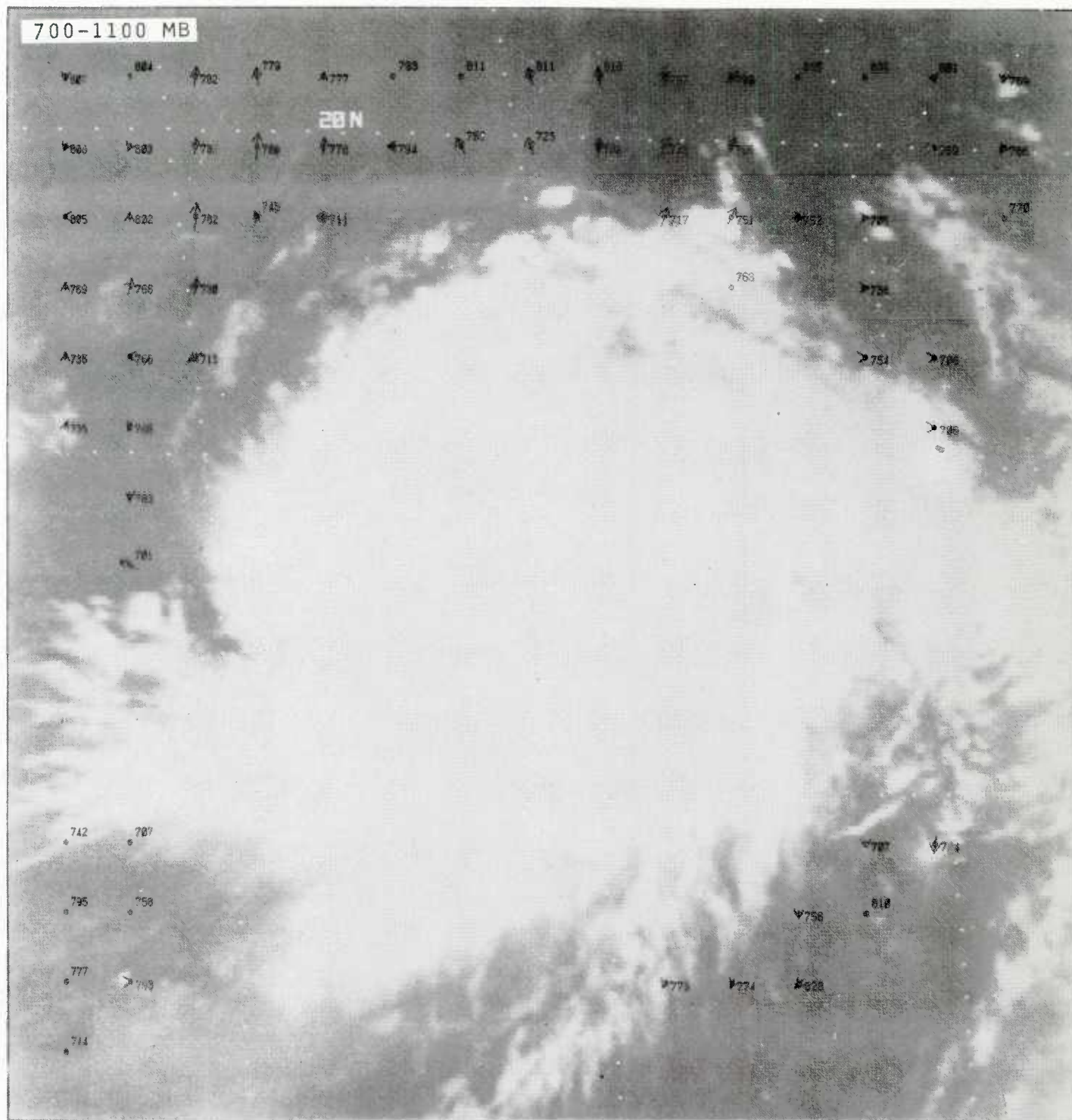


Figure 15c. Same as 15a and b, but for lower levels.

28 N

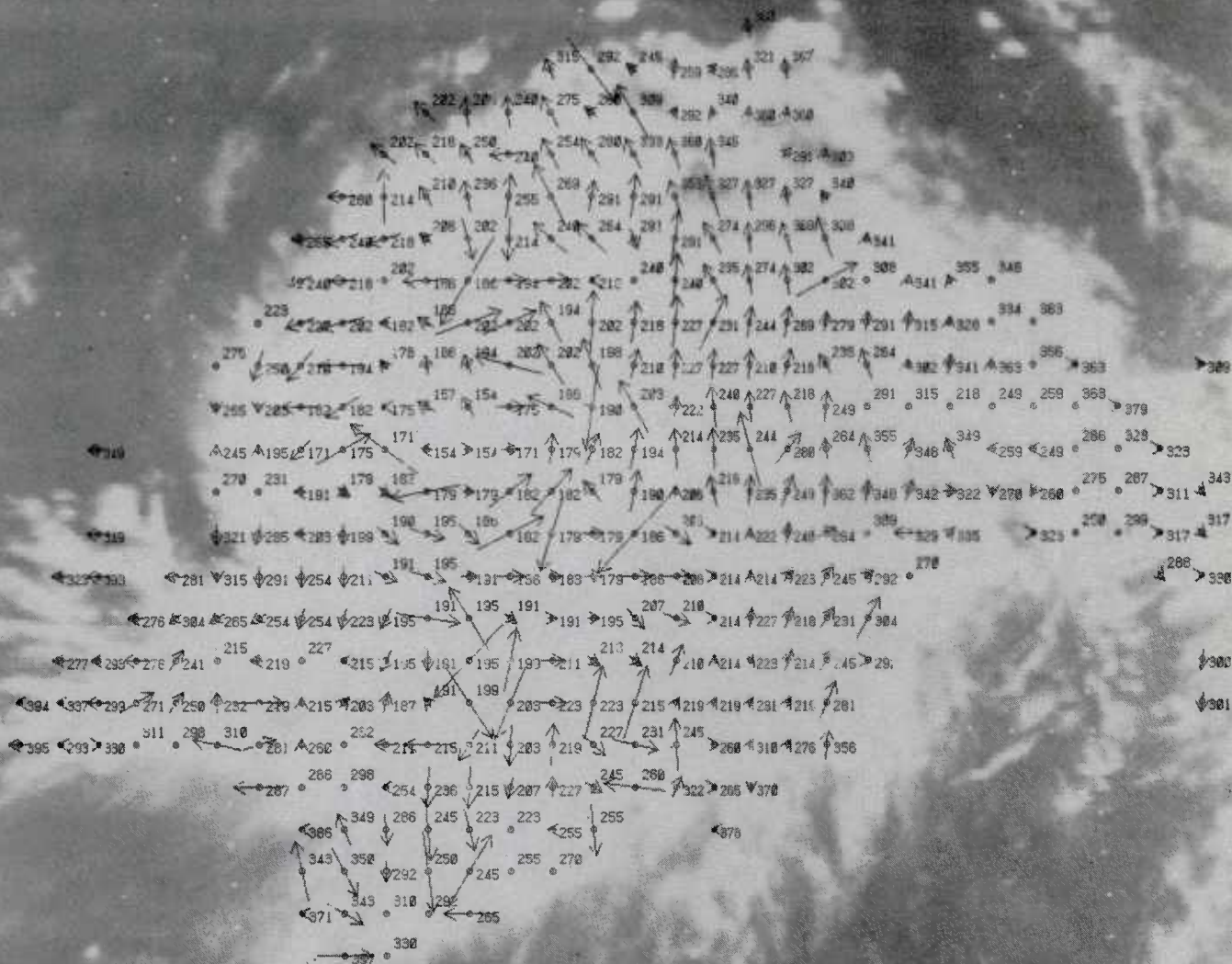


Figure 16. Same as 15a, but for a subarea size of 32 by 32 pixels with a 16 pixel overlap of subareas.

0-500 MB

454 443 432 422 422 422 439 455 454 471 487 487 487 479 478 469 497
 451 449 437 427 418 395 427 443 468 468 468 476 484 474 471 454 477 482
 481 467 484 452 448 438 485 448 466 463 492 500 466 456 439 437 459
 486 473 479 456 426 425 442 458 476 419 418 400 406 411 423 406 421
 397 396 397 399

378
 324 337
 294 316 328 354 374
 317 349 335 347 334 347 353 311
 349 41 354 316 351 343 355 355 322 328 328 341
 332 321 337 356 355 347 330 338 338 332 322 341 329
 320 318 318 358 342 331 326 325 325 325

245 285 284 211 219 318
 458 455 453 460 429 408 363 362 348 362 301
 497 444 442 440 458 466 454 423 448 458 446 454 472 448 419 448 380
 461 478 446 435 433 451 439 437 475 443 442 458 438 473 408
 454 499 482

245 276 304
 249 269 383 291 427
 258 278 381 328 485

Figure 17a. Same as 11a, but for a subarea size of 64 by 64 pixels with a 16 pixel overlap of subareas.

500-800 MB

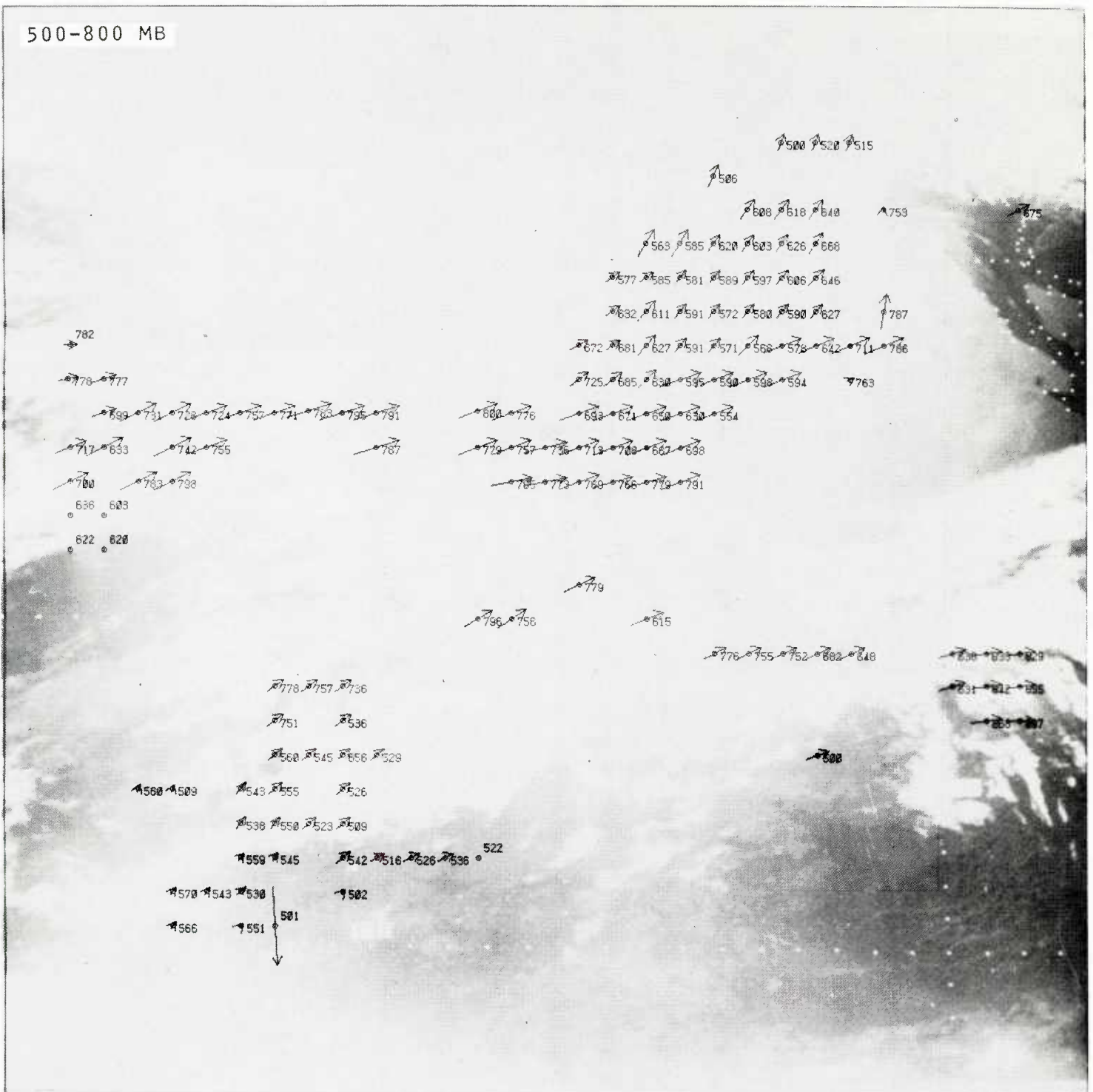


Figure 17b. Same as 11b, but for a subarea size of 64 by 64 pixels with a 16 pixel overlap of subareas.

800-1100 MB

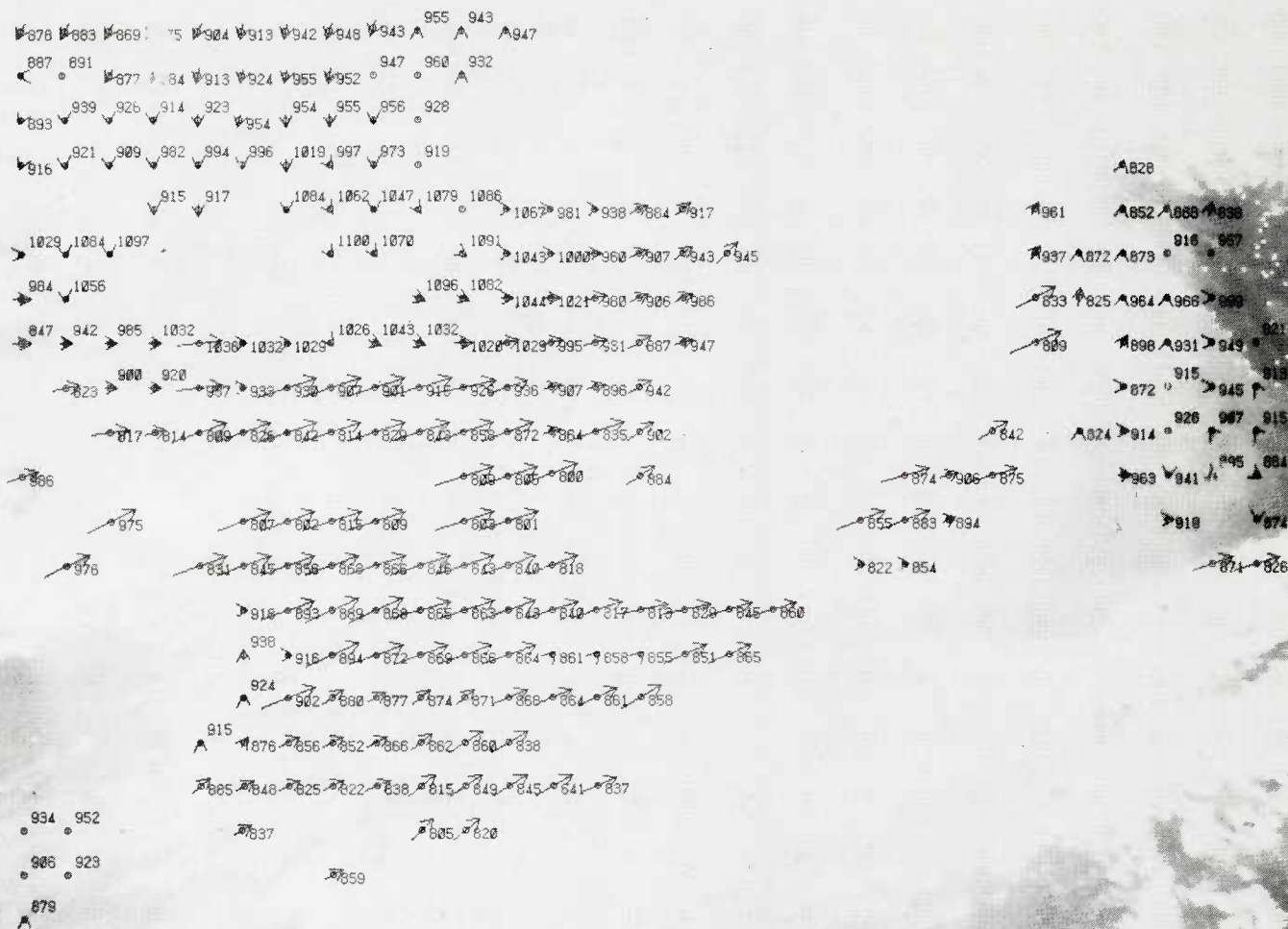


Figure 17c. Same as 11c, but for a subarea size of 64 by 64 pixels with a 16 pixel overlap of subareas.

5. DISCUSSION AND CONCLUSIONS

The SAWEGS embodies several unique aspects incorporated to address the problems in and to take advantage of specific characteristics of the XCOV cloud tracking method, and of automatic tracking in general. These aspects include histogram slicing, cloud edge and surface enhancement, multiple passes through the data, trackability tests, variable subarea sizes, and the use of numerical analysis temperature profiles in height assignment.

SAWEGS includes a histogram slicing technique to limit tracking to one distinct motion in each subarea. This technique adds an element of fine tuning to computed displacements by eliminating other than the dominant motion. In cases of multiple motions, particularly when the lower clouds are uniform cloud masses, a wind estimate which represents an average of the motions can result. Other problems involve the XCOV computation's tendency to track "holes" left by eliminating upper level clouds when slicing for lower clouds, and occasional inferior displacements produced with very narrow slicing ranges. However, in general, slicing is effective, and in some specific cases such as the visible case described in this report, slicing correctly identifies the motion of cirrus above clouds with contrasting motions.

For infrared data, truncation of high-order data bits provides improved displacement estimates by enhancing cloud edges and patterns. Inspection of individual subareas reveals that the best quality vectors are derived in subareas where truncation produces a high level of contrast. Because some subareas contain ranges of values that do not span multiples of 64 counts and thus do not benefit from truncation, further improvement may be made by developing methods of enhancement in these subareas.

Because development of an automatic cloud tracking system which produces a perfect vector in each subarea is an unattainable goal, the philosophy throughout the generation of the SAWEGS has been to produce the best possible set of vectors and then to rely on an effective quality control procedure to eliminate incorrect

vectors. The SAWEGS includes a capability for multiple passes through the images with a shift in subarea positions on each pass to assure that a sufficient number of correct vectors are available to overcome the influence of incorrect vectors.

Various tests applied throughout the wind extraction process prevent tracking in subareas with characteristics that show a high risk of producing a deficient cloud displacement. For the data cases presented in this report, these tests prevented tracking of between 0 and 35 percent of the total possible vectors. In some cases calm winds result from tracking subareas with no moving cloud elements. However, these calm winds are preferable to having no calm areas, characteristic of manually tracked vector sets.

Despite the lack of an emissivity correction, use of numerical analysis temperature profiles for determining the height assignment of derived vectors produces heights of good relative agreement. Subjective inspection suggests that heights are consistently underestimated, a characteristic that was somewhat alleviated by modifying the program to use an average IR value instead of the histogram peak used previously.

Height assignment of cloud motion vectors has received a large amount of attention in the past, but the accuracy of most height assignment algorithms remains little better than a capability to indicate high and low level vectors. While methods of actively modifying vector heights at the time of numerical assimilation (Lee, 1979) may improve the accuracy somewhat, height assignments must be considered only as estimates until more information can be supplied from space-borne sensors.

For an image set with given horizontal and temporal resolutions, the use of the optimum subarea size for extracting winds is extremely important; most of the tracking problems mentioned here are eliminated when these three quantities are in proper balance. The SAWEGS subarea size is variable so that the smallest possible subarea size that still allows for the greatest possible cloud movement in a set of images can be used. For an 8 km image resolution with 30 minute data, the optimum subarea size is 32 by 32 elements. This size is a compromise; a smaller subarea produces

more vectors, but allows clouds in one subarea in the first image to move into a different subarea in the second image. A subarea size of 32x32 elements near the equator will theoretically prevent clouds with speeds up to 142 m/s (32 elements x 8 km/30 min) from moving through the subarea, with greater speeds at higher latitudes. However, these values are reduced to between 70 m/s and 100 m/s by limiting each displacement to one quadrant of the XCOV matrix in response to the origin determination problem.

Utilizing the proper balance also limits the horizontal resolution which may be used for a given temporal resolution; a 32 by 32 subarea size for images of 4 km resolution results in a decrease in vector accuracy. Rogers et al (1979) called for tracking rapidly changing clouds around tropical cyclones using short time interval data sets to increase the quality of resulting vectors. Time intervals of 15, 7.5, or 3 minutes which proved effective in their experimentation are needed for producing finer scale wind sets with SAWEGS.

This fully automatic extraction of cloud motion vectors is extremely fast. One 512 by 512 element image region, without quality control or plotting, uses about 2.5 minutes of CPU time on a Control Data Corporation CYBER-175 computer.

Although some difficulties remain, the quality of the SAWEGS winds indicate the system's potential once these difficulties are overcome. Successful extraction of upper level winds with infrared data is particularly satisfying. Correct portrayal of various synoptic features, an ability to accurately track stratocumulus cells in visible data, and success with a difficult tropical cyclone case are other strengths of this system.

6. CONTINUED DEVELOPMENT

Development of SAWEGS continues toward solving remaining problems and including further capabilities. Completion of the quality control program, overcoming difficulties with the slicing technique, upgrading the height assignment method, and modifying the truncation enhancement to best enhance each subarea are major areas of work.

Other plans include coupling visible and infrared data during tracking. Using the two types of data, the optimum tracers in a subarea can be better determined by computing and analyzing bi-dimensional histograms as is done in the European Space Agency system (Bizzarri and Tomassini, 1976; Tomassini, 1980). Using the infrared data to compute heights for vectors extracted from visible data, and intercomparing vectors from the visible and the infrared for consistency are other elements of this plan.

Computing and then averaging vectors for two consecutive 30-minute periods is also planned, as is investigation of better positioning methods and interpolation of the peak within the XCOV matrix to gain subgrid scale accuracy in resulting winds.

Finally, plans include a study of the response of the XCOV algorithm to various conditions such as shape and brightness changes, simple translation, multiple motions, etc. By better understanding the XCOV algorithm, improvement in the quality of SAWEGS-produced vectors should continue.

ACKNOWLEDGMENTS

The authors appreciate the assistance of DM1 Frank Hermoso in graphics, PH1 Al Matthews in photography, Ms. Winona Carlisle in typing, and Mr. Stephen Bishop in editing for this report.

REFERENCES

- Arking, Albert, Robert C. Lo, and Azriel Rosenfeld, 1978: A Fourier approach to cloud motion estimation, J. Appl. Meteor., 17, 735-744.
- Austin, G. L., 1980: Personal communication.
- Austin, G. L., and A. Bellon, 1974: The use of digital weather radar records for short-term precipitation forecasting. Quart. J. R. Met. Soc., 100, 658-664.
- Bellon, A., and G. L. Austin, 1978: The evaluation of two years of real-time operation of a short-term precipitation forecasting procedure (SHARP). J. Appl. Meteor., 17, 1778-1787.
- Bizzarri, B. and Tomassini, C., 1976: Retrieval of information from high-resolution images. Proceedings of the Symposium on Meteorological Observations from Space: Their Contributions of the FGGE, COSPAR XIX, Philadelphia, Pennsylvania, June 8-10, 1976, 140-144.
- Bowen, R. A., L. Fusco, J. Morgan, and K. O. Roska, 1980: Operational production of cloud motion vectors (satellite winds) from METEOSAT image data. In The METEOSAT Central Processing System, Issue 2, March 1980, European Space Agency.
- Endlich, R. M., D. E. Wolf, D. J. Hall, and A. E. Bran, 1971: Use of a pattern recognition technique for determining cloud motions from sequences of satellite photographs. J. Appl. Meteor., 10, 105-117.
- European Space Agency, 1978: METEOSAT, meteorological users' handbook. Compiled by the Meteorological Information Extraction Centre of the METEOSAT Data Management Department, 13 Chapters.
- Green, R., G. Hughes, C. Novak, and R. Schertz, 1975: The automatic extraction of wind estimates from VISSR data. Central Processing and Analysis of Geostationary Satellite Data, NOAA Technical Memorandum NESS-64, 94-110.
- Hubert, Lester, F., 1979: Wind derivation from geostationary satellites. In Quantitative Meteorological Data from Satellites, World Meteorological Organization Technical Note No. 66, edited by Jay S. Winston, 33-59.
- Lee, David H., 1979: Level assignment in the assimilation of cloud motion vectors. Mon. Wea. Rev., 107, 1055-1074.

- Leese, John A., Charles S. Novak, and Bruce B. Clark, 1971: An automated technique for obtaining cloud motion from geosynchronous satellite data using cross correlation. J. Appl. Meteor., 10, 118-132.
- Lo, Robert C., and Jeffrey Mohr, 1974: Applications of enhancement and thresholding techniques to Fourier transform cloud motion estimation. University of Maryland Technical Report TR-326, 30 pp.
- Nagle, R. E., and D. H. Lee, 1979: Automated cloud-tracking using GOES imagery. In Proceedings of the 8th Technical Exchange Conference, Air Force Academy, Colorado, 28 November-1 December 1978, 105-111.
- Novak, C., and M. Young, 1977: The operational processing of wind estimates from cloud motions: Past, present and future. Proceedings of Eleventh International Symposium on Remote Sensing of the Environment, Ann Arbor, Michigan, 1589-1598.
- Rodgers, Edward, R. Cecil Gentry, William Shenk, and Vincent Oliver, 1979: The benefits of using short-interval satellite images to derive winds for tropical cyclones. Mon. Wea. Rev. 107, 575-584.
- Thomasell, Albert, Jr., 1979: Personal communication.
- Tomassini, C., 1980: Objective classification technique in METEOSAT image data processing. In The METEOSAT central processing system, Issue 2, March 1980, European Space Agency.
- Weinstein, F. S., 1972: An advantageous method of performing cross-correlational analysis. Proceedings of IEEE, 60, 449-450.
- Westinghouse, Electric Corporation, 1977: Earth location equations. Westinghouse Electric Corporation, Defense and Electronic Systems Center, report to National Aeronautics and Space Administration on contract NAS 5-23582, 21 pp.
- Wilson, Gregory S., 1980: Personal communication.
- Wolf, D. E., and R. M. Endlich, 1980: Application of the SRI cloud tracking technique to rapid-scan GOES observations. Final Report, Contract NAS 5-25027, SRI International, Menlo Park, California, 26 pp.
- Wolf, D. E., D. J. Hall, and R. M. Endlich, 1977: Experiments in automatic cloud tracking using SMS-GOES data. J. Appl. Meteor. 16, 1219-1230.

APPENDIX A: SLICING TECHNIQUE EVOLUTION

The slicing technique described in Section 3.1.2 evolved through many stages of development. Some ideas for improving the technique were tested but not implemented for various reasons. Because an awareness of the problems with these ideas is important, a few will be discussed here.

Originally the slicing technique produced and tracked multiple slices in each subarea. Instead of selecting only the maximum distribution peak, slices around all peaks were identified and a vector derived for each. A similar technique called "thresholding" is suggested by Lo and Mohr (1974). Such a technique theoretically should produce a different vector for each motion evident in a particular subarea. In practice, however, the vectors derived for the respective slices are nearly identical to each other. This contradiction appears to occur because the XCOV computation is affected by the zeroed-out areas outside the slice as well as by the clouds within the slice.

In an attempt to negate or reduce the effects of the area outside the slice, various treatments of the background were tried. These treatments replaced each subarea element outside the slicing range with one of the following six values:

- 1) a random count value,
- 2) the mean value of counts within the slice, .
- 3) one less than the lower slice limit,
- 4) zero below the slicing limit and 255 (the maximum possible count value) above the limit,
- 5) one less than the lower slice limit for image values below the slicing limit and one more than the upper slice limit for values above the slicing limit, or
- 6) zero, while setting all values within the slice limits to 255.

Unfortunately, none of these treatments enable the multiple slicing to produce vectors representing other than the dominant motion.

Another modification to the slicing tested a reduction in the slice limits. Suggested by Thomasell (1979), this reduction is designed to eliminate the zone on the edges of clouds where most

of the variance in the slice count values has been observed. A percentage of the total number of image elements in the slice is used to narrow the upper and lower slice count limits. The use of a standard deviation of the slice around the peak to reduce the slice was also tested. Neither of these techniques showed significant improvement in the resulting vector field when compared with the cloud movements evident in satellite images.

Slicing of another type was also tested with infrared data, slicing based on predetermined pressure height limits instead of the count distribution. Standard pressure values for low, middle, and high level clouds were specified as slice limits. Using a technique which is the inverse of that applied to determine height assignments (described in Section 3.3), these pressure limits were transformed into image counts and the slicing performed as before. Because this slicing method could conceivably result in throwing away much of the tracking information in a subarea, the method was abandoned in favor of slicing based on the image distributions.

APPENDIX B: XCOV MATRIX ORIGIN DETERMINATION DEVELOPMENT

Before implementing the technique described in Section 3.2.2, a number of methods were tested to determine which XCOV matrix origin gives the correct vector displacement. Most methods computed a first guess displacement vector in some way, then selected the origin giving a result closest to the first guess' directional component. First guesses used included:

- 1) the displacement in the element of maximum image count between images,
- 2) the displacement in the centroid of the area retained after slicing,
- 3) an objective analysis of SAWEGS vectors with half the horizontal resolution; the "guess" run of SAWEGS assumed the origin closest to the matrix maximum, and
- 4) objective analyses as for the previous guess but for low, middle, and high levels, separately.

Each of these first guesses gave an increasing number of correctly determined displacements. However, even the rather complex use of an objective analysis at each level of a "guess" SAWEGS vector set failed to identify the correct origin in approximately 15 percent of the subareas.

A simpler method of origin determination, which does not involve the use of a first guess, was ultimately included in SAWEGS.

DISTRIBUTION

COMMANDER IN CHIEF
U.S. PACIFIC FLEET
PEARL HARBOR, HI 96860

COMMANDER
SEVENTH FLEET (N30W)
ATTN: FLEET METEOROLOGIST
FPO SAN FRANCISCO 96601

COMMANDER
NAVAL SURFACE FORCE
U.S. PACIFIC FLEET
CODE N331A
NAVAL AMPHIBIOUS BASE
SAN DIEGO, CA 92155

COMMANDER
AMPHIBIOUS GROUP 1
ATTN: METEOROLOGICAL OFFICER
FPO SAN FRANCISCO 96601

OFFICER IN CHARGE
OPERATIONAL TEST & EVALUATION
FORCE, SUNNYVALE
NAVAL AIR STATION
MOFFETT FIELD, CA 94035

COMMANDER
U.S. NAVAL SUPPORT FORCE
ANTARCTICA
FPO SAN FRANCISCO 96601

COMMANDER
SURFACE WARFARE DEVELOPMENT GRP.
NAVAL AMPHIBIOUS BASE, LITTLE CREEK
NORFOLK, VA 23521

COMMANDER NAVAL SURFACE GROUP
WESTERN PACIFIC
FPO SAN FRANCISCO 96601

COMMANDING OFFICER
USS FORRESTAL (CV-59)
ATTN: METEOROLOGICAL OFFICER
FPO MIAMI 34080

COMMANDING OFFICER
USS INDEPENDENCE (CV-62)
ATTN: METEOROLOGICAL OFFICER
FPO NEW YORK 09537

COMMANDING OFFICER
USS NIMITZ (CVN-68)
ATTN: METEOROLOGICAL OFFICER
FPO NEW YORK 09542

COMMANDING OFFICER
USS CONSTELLATION (CV-64)
ATTN: METEOROLOGICAL OFFICER
FPO SAN FRANCISCO 96635

COMMANDING OFFICER
USS ENTERPRISE (CVN-65)
ATTN: METEOROLOGICAL OFFICER
FPO SAN FRANCISCO 96636

COMMANDING OFFICER
USS KITTY HAWK (CV-63)
ATTN: METEOROLOGICAL OFFICER
FPO SAN FRANCISCO 96634

COMMANDING OFFICER
USS MIDWAY (CV-41)
ATTN: METEOROLOGICAL OFFICER
FPO SAN FRANCISCO 96631

COMMANDING OFFICER
SARATOGA NUCLEUS CREW
ATTN: METEOROLOGICAL OFFICER
FPO NEW YORK 09501

COORDINATOR
NATIONAL ATMOSPHERIC RSCH PROGRAM
INSTITUTE OF PHYSICS
ACADEMIA SINICA
TAIPEI, TAIWAN

COMMANDING OFFICER
USS GUADALCANAL (LPH-7)
ATTN: METEOROLOGICAL OFFICER
FPO NEW YORK 09562

COMMANDING OFFICER
USS GUAM (LPH-9)
ATTN: METEOROLOGICAL OFFICER
FPO NEW YORK 09563

COMMANDING OFFICER
USS INCHON (LPH-12)
ATTN: METEOROLOGICAL OFFICER
FPO NEW YORK 09529

COMMANDING OFFICER
USS IWO JIMA (LPH-2)
ATTN: METEOROLOGICAL OFFICER
FPO NEW YORK 09561

COMMANDING OFFICER
USS NEW ORLEANS (LPH-11)
ATTN: METEOROLOGICAL OFFICER
FPO SAN FRANCISCO 96627

COMMANDING OFFICER
USS LEXINGTON (AVT-16)
FPO MIAMI 34088

AVIATION SUPPORT DEPT. OFFICER
NSFA, DETACHMENT CHRISTCHURCH
ANTARCTIC DEV. SQUADRON 6-VXE-6
FPO SAN FRANCISCO 96690

SACLANT
ASW RESEARCH CENTER
APO NEW YORK 09019

SPECIAL ASST. TO THE ASST.
SECRETARY OF THE NAVY (R&D)
ROOM 4F741
THE PENTAGON
WASHINGTON, DC 20350

CHIEF OF NAVAL RESEARCH
LIBRARY SERVICES (CODE 734)
RM 633, BALLSTON TOWER #1
800 QUINCY STREET
ARLINGTON, VA 22217

OFFICE OF NAVAL RESEARCH
CODE 465
ARLINGTON, VA 22217

DR. R. W. JAMES
OPNAV 95201
U.S. NAVAL OBSERVATORY
34th & MASSACHUSETTS AVE, N.W.
WASHINGTON, DC 20390

CHIEF OF NAVAL MATERIAL
(MAT-034)
NAVY DEPARTMENT
WASHINGTON, DC 22332

NAVAL DEPUTY TO THE
ADMINISTRATOR, NOAA
ROOM 200, PAGE BLDG. #1
3300 WHITEHAVEN ST. NW
WASHINGTON, DC 20235

OFFICER IN CHARGE
NAVOCEANCOMDET
NAVAL STATION
FPO SEATTLE 98791

OFFICER IN CHARGE
US NAVOCEANCOMDET
BOX 81
U.S. NAVAL AIR STATION
FPO SAN FRANCISCO 96637

CENTRAL WX BUREAU
64, KUNG YUAN RD
TAIPEI, TAIWAN 100

DEPARTMENT OF ATMOS. SCIENCE
NATIONAL TAIWAN UNIVERSITY
TAIPEI, TAIWAN 107

OFFICER IN CHARGE
NAVOCEANCOMDET
U.S. NAVAL AIR FACILITY
FPO SEATTLE 98767

CHIEF PETTY OFFICER IN CHARGE
NAVOCEANCOMDET
CHASE FIELD
BEEVILLE, TX 78103

OFFICER IN CHARGE
NAVOCEANCOMDET
NAVAL AIR STATION
CORPUS CHRISTI, TX 78419

OFFICER IN CHARGE
US NAVOCEANCOMDET
BOX 63
U.S. NAVAL AIR STATION
FPO SAN FRANCISCO 96654

OFFICER IN CHARGE
NAVOCEANCOMDET
BOX 9048
NAVAL AIR STATION
KEY WEST, FL 33040

CHIEF PETTY OFFICER IN CHARGE
NAVOCEANCOMDET
NAVAL AIR STATION
KINGSVILLE, TX 78363

OFFICER IN CHARGE
NAVOCEANCOMDET
NAVAL AIR STATION
WHITING FIELD
MILTON, FL 32570

OFFICER IN CHARGE
NAVOCEANCOMDET
NAVAL AIR STATION
MERIDIAN, MS 39301

OFFICER IN CHARGE
NAVOCEANCOMDET
NAVAL AIR STATION
MOFFETT FIELD, CA 94035

OFFICER IN CHARGE
US NAVOCEANCOMDET
NAPLES, BOX 23
FPO NEW YORK 09520

OFFICER IN CHARGE
NAVOCEANCOMDET
AFGWC
OFFUTT AFB, NE 68113

OFFICER IN CHARGE
NAVOCEANCOMDET
NAVAL AIR STATION
PATUXENT RIVER, MD 20670

OFFICER IN CHARGE
NAVOCEANCOMDET
U.S. NAVAL STATION
FPO MIAMI 34051

OFFICER IN CHARGE
NAVOCEANCOMDET
U.S. NAVAL AIR FACILITY
FPO NEW YORK 09523

OFFICER IN CHARGE
NAVOCEANCOMDET
NAVAL AIR STATION, OCEANA
VIRGINIA BEACH, VA 23460

OFFICER IN CHARGE
NAVOCEANCOMDET
NAVAL AIR STATION
WILLOW GROVE, PA 19090

METEOROLOGICAL DEPT.
BOX 200 LUSAKA
ZAMBIA

METEOROLOGICAL SATELLITE
CENTER
235 NAKAKIYOT 3-CHROME
KIYOSE, TOKYO 180-04
JAPAN

OFFICER IN CHARGE US NAVOCEANCOMDET FPO SAN FRANCISCO 96685	COMMANDING OFFICER NAVOCEANCOMFAC NAVAL AIR STATION, NORTH ISLAND SAN DIEGO, CA 92135	LIBRARY NAVAL POSTGRADUATE SCHOOL MONTEREY, CA 93940
OFFICER IN CHARGE US NAVOCEANCOMDET FLEET ACTIVITIES FPO SEATTLE 98770	COMMANDING OFFICER US NAVOCEANCOMFAC FPO SEATTLE 98762	COMMANDING OFFICER ATTN: WEATHER SERVICE OFFICE MARINE CORPS AIR STATION KANEHOE BAY, HI 96863
COMMANDING OFFICER NAVAL RESEARCH LAB ATTN: LIBRARY, CODE 2620 WASHINGTON, DC 20390	CHAIRMAN OCEANOGRAPHY DEPT. U.S. NAVAL ACADEMY ANNAPOLIS, MD 21402	COMMANDING GENERAL ATTN: WEATHER SERVICE OFFICE MARINE CORPS AIR STATION EL TORO SANTA ANA, CA 92709
COMMANDING OFFICER OFFICE OF NAVAL RESEARCH 1030 E. GREEN STREET PASADENA, CA 91101	COMMANDER NAVAIRSYSCOM ATTN: LIBRARY (AIR-00D4) WASHINGTON, DC 20361	COMMANDING OFFICER ATTN: WEATHER SERVICE OFFICE MARINE CORPS AIR STATION YUMA, AZ 85364
OFFICE OF NAVAL RESEARCH SCRIPPS INSTITUTION OF OCEANOGRAPHY LA JOLLA, CA 92037	COMMANDER NAVAIRSYSCOM AIR-370 WASHINGTON, DC 20361	COMMANDER AWS/DN SCOTT AFB, IL 62225
COMMANDING OFFICER NORDA, CODE 101 NSTL STATION BAY ST. LOUIS, MS 39529	COMMANDER NAVAIRSYSCOM METEOROLOGICAL SYSTEMS DIV. AIR-553 WASHINGTON, DC 20360	3350TH TECHNICAL TRNG GROUP TTGU-W/STOP 623 CHANUTE AFB, IL-61868
COMMANDER NAVAL OCEANOGRAPHY COMMAND NSTL STATION BAY ST. LOUIS, MS 39529	COMMANDER NAVAIRSYSCOM, AIR-03 ATTN: CAPT C.M. RIGSBEE WASHINGTON, DC 20361	AFGL/LY HANSCOM AFB, MA 01731
COMMANDING OFFICER NAVAL OCEANOGRAPHIC OFFICE NAVY LIBRARY NSTL STATION BAY ST. LOUIS, MS 39522	COMMANDER ATTN: CODE 032 NAVFACENGCOM, RESEARCH DIV. 200 STOVALL ST. ALEXANDRIA, VA 22332	AFGL/OPI HANSCOM AFB, MA 01731
COMMANDING OFFICER FLENUMOCEANCEN MONTEREY, CA 93940	COMMANDER NAVAL OCEAN SYSTEMS CENTER ATTN: CODE 4473 SAN DIEGO, CA 92152	5WW/DN LANGLEY AFB, VA 23665
OFFICER IN CHARGE NAVOCEANCOMDET C/O FLENUMOCEANCEN MONTEREY, CA 93940	COMMANDER EARTH & PLANETARY SCIENCES CODE 3918 NAVAL WEAPONS CENTER CHINA LAKE, CA 93555	OFFICER IN CHARGE SERVICE SCHOOL COMMAND DET. CHANUTE/STOP 62 CHANUTE AFB, IL 61868
COMMANDING OFFICER NAVWESTOCEANCEN BOX 113 PEARL HARBOR, HI 96860	COMMANDER NAVAL SHIP RSCH & DEV CENTER CODE 5220 BETHESDA, MD 20084	1ST WEATHER WING (DON) HICKAM AFB, HI 96853
COMMANDING OFFICER NAVEASTOCEANCEN MCADIE BLDG. (U-117) NAVAL AIR STATION NORFOLK, VA 23511	COMMANDER ATTN: DR. B. KATZ WHITE OAKS LAB NAVAL SURFACE WEAPONS CENTER SILVER SPRING, MD 20910	DET 4 HQ AWS/CC APO SAN FRANCISCO 96334
COMMANDING OFFICER NAVPOlarOCEANCEN NAVY DEPT. 4301 SUITLAND RD. WASHINGTON, DC 20390	NAVAL SPACE SYSTEMS ACTIVITY CODE 60 P.O. BOX 92960 WORLDWAY POSTAL CENTER LOS ANGELES, CA 90009	DET 8, 30 WS APO SAN FRANCISCO 96239
COMMANDING OFFICER US NAVOCEANCOMCEN BOX 12 COMNAVMAIANAS FPO SAN FRANCISCO 96630	COMMANDER PACIFIC MISSILE TEST CENTER ATTN: GEOPHYSICS OFFICER CODE 3250 PT. MUGU, CA 93042	AFOSR/NC BOLLING AFB WASHINGTON, DC 20312
COMMANDING OFFICER US NAVOCEANCOMCEN BOX 31 FPO NEW YORK 09540	DEPT. OF METEOROLOGY NAVAL POSTGRADUATE SCHOOL MONTEREY, CA 93940	OFFICE OF STAFF METEOROLOGY WESTERN SPACE & MISSILE CENTER (WE) VANDENBERG AFB, CA 93437
COMMANDING OFFICER OCEANCOMFAC P.O. BOX 85 NAVAL AIR STATION JACKSONVILLE, FL 32212	DEPT. OF OCEANOGRAPHY NAVAL POSTGRADUATE SCHOOL MONTEREY, CA 93940	COMMANDER & DIRECTOR ATTN: DELAS-DM-A U.S. ARMY ATMOS. SCIENCES LAB WHITE SANDS MISSILE RANGE WHITE SANDS, NM 88002
COMMANDING OFFICER OFFICE OF NAVAL RESEARCH EASTERN/CENTRAL REGIONAL OFFICE, BLDG 114 SECT. D 666 SUMMER ST. BOSTON, MA 02210		COMMANDING OFFICER U.S. ARMY RESEARCH OFFICE ATTN: GEOPHYSICS DIV. P.O. BOX 12211 RESEARCH TRIANGLE PARK, NC 27709
		DIRECTOR DEFENSE TECH. INFORMATION CENTER CAMERON STATION ALEXANDRIA, VA 22314
		DIRECTOR OFFICE OF ENV. & LIFE SCI. OFFICE OF UNDERSECRETARY OF DEFENSE FOR RSCH & ENG (E&LS) ROOM 3D129, THE PENTAGON WASHINGTON, DC 20301

CHIEF
MARINE SCIENCE SECTION
U.S. COAST GUARD ACADEMY
NEW LONDON, CT 06320

COMMANDING OFFICER
U.S. COAST GUARD
OCEANOGRAPHIC UNIT
BLDG 159-E
WASHINGTON NAVY YARD
WASHINGTON, DC 20390

COMMANDING OFFICER
USCG RESEARCH & DEVELOPMENT CENTER
GROTON, CT 06340

DIRECTOR
SYSTEMS DEVELOPMENT
NWS/NOAA
ROOM 1216 - THE GRAMAX BLDG
8060 13TH STREET
SILVER SPRING, MD 20910

DEVELOPMENT DIVISION
NATIONAL METEOROLOGICAL CENTER
NWS/NOAA
WORLD WEATHER BLDG. W32, RM 204
WASHINGTON, DC 20233

DIRECTOR
NATIONAL EARTH SAT. SERV/SEL
FB-4, S321B
SUITLAND, MD 20233

ACQUISITIONS SECTION
IRDB-D823
LIBRARY & INFO. SERV. DIV.
NOAA, 6009 EXECUTIVE BLVD.
ROCKVILLE, MD 20852

FEDERAL COORDINATOR FOR
METEOR. SERV. & SUP. RSCH.
6010 EXECUTIVE BLVD
ROCKVILLE, MD 20852

DIRECTOR
OFFICE OF PROGRAMS RX3
NOAA RSCH LABS
BOULDER, CO 80302

DIRECTOR
NATIONAL HURRICANE CENTER
NOAA, UNIV. OF MIAMI BRANCH
CORAL GABLES, FL 33124

NATIONAL WEATHER SERVICE
WORLD WEATHER BLDG.
ROOM 307
5200 AUTH ROAD
CAMP SPRINGS, MD 20023

DIRECTOR
NATIONAL SEVERE STORMS LAB
1313 HALLEY CIRCLE
NORMAN, OK 73069

NATIONAL WEATHER SERVICE,
EASTERN REGION
ATTN: WFE3
585 STEWART AVE.
GARDEN CITY, NY 11530

CHIEF, SCIENTIFIC SERVICES
NWS, CENTRAL REGION
NOAA, ROOM 1836
601 EAST 12TH STREET
KANSAS CITY, MO 64106

CHIEF, SCIENTIFIC SERVICES
NWS, SOUTHERN REGION
NOAA, ROOM 10F09
819 TAYLOR STREET
FT. WORTH, TX 76102

CHIEF, SCIENTIFIC SERVICES
NWS, PACIFIC REGION
P.O. BOX 50027
HONOLULU, HI 96850

NOAA RESEARCH FACILITIES CENTER
P.O. BOX 520197
MIAMI, FL 33152

CHIEF, OPERATIONS BRANCH
AIR RESOURCES LAB, NOAA
P.O. BOX 14985 AEC
LAS VEGAS, NV 89114

DIRECTOR
ATLANTIC OCEANO & METEOR LABS
15 RICKENBACKER CAUSEWAY
VIRGINIA KEY
MIAMI, FL 33149

DIRECTOR
GEOPHYSICAL FLUID DYNAMICS LAB
NOAA, PRINCETON UNIVERSITY
P.O. BOX 308
PRINCETON, NJ 08540

NATIONAL MARINE FISHERIES SERV.
OCEAN CLIMATOLOGY PROJECT
SOUTHWEST FISHERIES CENTER
P.O. BOX 271
LA JOLLA, CA 92037

DR. MICHAEL HELFERT
SF-NOAA LIAISON MANAGER
NASA-JOHNSON SPACE CENTER
HOUSTON, TX 77058

CHIEF
MESOSCALE APPLICATIONS BRANCH
NATIONAL EARTH SATELLITE SERV.
1225 WEST DAYTON
MADISON, WI 53562

HEAD, ATMOS. SCIENCES DIV.
NATIONAL SCIENCE FOUNDATION
1800 G. STREET, NW, Rm. 644
WASHINGTON, DC 20550

LABORATORY FOR ATMOS. SCI.
NASA GODDARD SPACE FLIGHT
CENTER
GREENBELT, MD 20771

PRELIMINARY SYSTEMS DESIGN
GROUP
NASA GODDARD SPACE FLIGHT
CENTER
GREENBELT, MD 20771

EXECUTIVE SECRETARY
CAO COMMITTEE ON ATMOS. SCI.
NATIONAL SCIENCE FOUNDATION
ROOM 510
1800 G STREET NW
WASHINGTON, DC 20550

NATIONAL CENTER FOR ATMOS. RSCH
LIBRARY ACQUISITIONS
P.O. BOX 1470
BOULDER, CO 80302

DEPT. OF ATMOSPHERIC SCIENCES
ATTN: LIBRARIAN
COLORADO STATE UNIVERSITY
FORT COLLINS, CO 80521

CHAIRMAN
DEPT. OF METEOROLOGY
PENNSYLVANIA STATE UNIVERSITY
503 DEIKE BLDG.
UNIVERSITY PARK, PA 16802

CHAIRMAN
DEPARTMENT OF METEOROLOGY
MASSACHUSETTS INSTITUTE OF
TECHNOLOGY
CAMBRIDGE, MA 02139

ATMOSPHERIC SCIENCES DEPT.
UNIVERSITY OF CHICAGO
1100 E. 57TH STREET
CHICAGO, IL 60637

DIRECTOR
INSTITUTE OF GEOPHYSICS
UNIV. OF CALIFORNIA AT
LOS ANGELES
LOS ANGELES, CA 90024

ATMOSPHERIC SCIENCES DEPT.
UNIVERSITY OF WASHINGTON
SEATTLE, WA 98195

CHAIRMAN
DEPT. OF METEOROLOGY &
OCEANOGRAPHY
4072 EAST ENGINEERING BLDG.
THE UNIVERSITY OF MICHIGAN
ANN ARBOR, MI 48104

CHAIRMAN
DEPARTMENT OF METEOROLOGY
UNIVERSITY OF WISCONSIN
METEOROLOGY & SPACE SCIENCE BLDG.
1225 WEST DAYTON STREET
MADISON, WI 53706

DIRECTOR
REMOTE SENSING LAB
P.O. BOX 248003
UNIVERSITY OF MIAMI
CORAL GABLES, FL 33124

ATMOSPHERIC SCIENCES DEPT.
OREGON STATE UNIVERSITY
CORVALLIS, OR-97331

CHAIRMAN
INSTITUTE OF ATMOS. PHYSICS
UNIVERSITY OF ARIZONA
TUSCON, AZ 85721

DEPT. OF METEOROLOGY
TEXAS A&M UNIVERSITY
COLLEGE STATION, TX 77843

DEAN OF THE COLLEGE OF SCIENCE
DREXEL INSTITUTE OF TECHNOLOGY
PHILADELPHIA, PA 19104

CHAIRMAN
DEPT. OF METEOROLOGY
UNIVERSITY OF OKLAHOMA
NORMAN, OK 73069

CHAIRMAN
DEPT. OF METEOROLOGY &
PHYSICAL OCEANO.
COOK COLLEGE,
P.O. BOX 231
RUTGERS UNIVERSITY
NEW BRUNSWICK, NJ 08903

CHAIRMAN
DEPT. OF ATMOSPHERIC SCIENCE
UNIV. OF MISSOURI, COLUMBIA
701 HITT STREET
COLUMBIA, MO 65211

DIRECTOR OF RESEARCH
INSTITUTE FOR STORM RSCH.
UNIVERSITY OF ST. THOMAS
3812 MONTROSE BLVD.
HOUSTON, TX 77006

CHAIRMAN
DEPARTMENT OF METEOROLOGY
CALIFORNIA STATE UNIV.
SAN JOSE, CA 95192

DOCUMENTS/REPORTS SECTION
LIBRARY
SCRIPPS INSTITUTE OF
OCEANOGRAPHY
LA JOLLA, CA 92037

LIBRARY
ATMOS. SCIENCES DEPT.
STATE UNIV. OF NEW YORK
1400 WASHINGTON AVE.
ALBANY, NY 12222

DIRECTOR
CENTER FOR MARINE STUDIES
SAN DIEGO STATE UNIVERSITY
SAN DIEGO, CA 92182

R.S.M.A.S. LIBRARY
UNIVERSITY OF MIAMI
4600 RICKENBACKER CAUSEWAY
VIRGINIA KEY
MIAMI, FL 33149

HEAD
DEPT. OF ENVIRONMENTAL SCI.
UNIV. OF VIRGINIA, CLARK HALL
ATTN: R. PIELKE
CHARLOTTESVILLE, VA 22903

CHAIRMAN
DEPT. OF ATMOSPHERIC SCI.
UNIVERSITY OF VIRGINIA
CLARK HALL
CHARLOTTESVILLE, VA 22903

DEPT. OF GEOGRAPHY
GUSTAVUS ADOLPHUS COLLEGE
ST. PETER, MN 56082

ATMOSPHERIC SCIENCES DEPT.
UCLA
405 HILGARD AVE.
LOS ANGELES, CA 90024

DEPT. OF ATMOS. SCI. LIBRARY
COLORADO STATE UNIVERSITY
FOOTHILLS CAMPUS
FT. COLLINS, CO 80523

DEPT. OF METEOROLOGY
UNIVERSITY OF MARYLAND
COLLEGE PARK, MD 20742

SAINT LOUIS UNIVERSITY
DEPT. OF EARTH & ATMOS. SCI.
P.O. BOX 8099 - LACLEDE STATION
ST. LOUIS, MO 63156

METEOROLOGY DEPT.
EASTERN AIR LINES, INC.
MIAMI INTERNATIONAL AIRPORT
MIAMI, FL 33148

WALTER A. BOHAN CO.
2026 OAKTON STREET
PARK RIDGE, IL 60068

METEOROLOGY INTERNATIONAL
2600 GARDEN RD.
MONTEREY, CA 93940

LIBRARY
THE RAND CORPORATION
1700 MAIN STREET
SANTA MONICA, CA 90406

DEPT. OF GEOPHYSICS & ASTRONOMY
THE RAND CORPORATION
1700 MAIN STREET
SANTA MONICA, CA 90406

METEOROLOGY DEPT.
UNITED AIR LINES
P.O. BOX 66100
CHICAGO, IL 60666

MANAGER
METEOROLOGICAL SERVICES
PAN AMERICAN AIRWAYS, HANGAR 14
JFK INTERNATIONAL AIRPORT
JAMAICA, NY 11430

CONTROL DATA CORP.
METEOROLOGY DEPT., RSCH DIV.
2800 E. OLD SHAKOPEE RD.
BOX 1249
MINNEAPOLIS, MN 55440

AEROSPACE CORPORATION
ATTN: METEOROLOGY SECTION
P.O. BOX 92957
LOS ANGELES, CA 90009

LFE ENVIRON. ANALYSIS LABS
2030 WRIGHT AVE.
RICHMOND, CA 94804

PRESIDENT
GEOATMOSPHERICS CORP.
BOX 177
LINCOLN, MA 01773

LABORATORY OF CLIMATOLOGY
ROUTE 1
CENTERTON
ELMER, NJ 08318

DIRECTOR OF METEOROLOGY
TRANS WORLD AIRLINES
HANGAR 12 - ROOM 235
J.F. KENNEDY INTERNATIONAL
AIRPORT
JAMAICA, NY 11430

SECTION MANAGER
LIBRARY
MCDONNELL-DOUGLAS CO.
P.O. BOX 516
ST. LOUIS, MO 63166

LIBRARY
GULF COAST RESEARCH LAB
OCEAN SPRINGS, MS 39564

SEA USE COUNCIL
1101 SEATTLE TOWER
SEATTLE, WA 98101

ENVIRONMENTAL RESEARCH &
TECHNOLOGY, INC.
696 VIRGINIA ROAD
CONCORD, MA 01742

OCEAN DATA SYSTEMS INC.
2460 GARDEN ROAD
MONTEREY, CA 93940

LEE W. PARKER, INC.
252 LEXINGTON RD.
CONCORD, MA 01742

LAGUNA RESEARCH LABS
21421 STANS LANE
LAGUNA BEACH, CA 92651

NAUTILUS PRESS, INC.
1056 NATIONAL PRESS BLDG.
WASHINGTON, DC 20045

UNIVERSAL MARINE, INC.
8222 TRAVELAIR ST.
HOUSTON, TX 77061

ATMOSPHERIC SCIENCE CENTER
SRI INTERNATIONAL
333 RAVENSWOOD AVE.
MENLO PARK, CA 94025

THE EXECUTIVE DIRECTOR
AMERICAN METEOROLOGICAL
SOCIETY
45 BEACON STREET
BOSTON, MA 02108

AMERICAN MET. SOCIETY
METEOROLOGICAL &
GEOASTROPHYSICAL ABSTRACTS
P.O. BOX 1736
WASHINGTON, DC 20013

WORLD METEOROLOGICAL ORGANIZATION
ATS DIVISION
ATTN: N. SUZUKI
CH-1211, GENEVA 20
SWITZERLAND

SERVÍCIO METEOROLÓGICO
DE LA ARMADA
EDIFICIO LIBERTAD, PISO 15
COMODORO PY Y CORBETA URUGUAY (1104)
BUENOS AIRES
REPUBLICA ARGENTINA

DIRECTOR GENERAL
SERVICIO METEOROLÓGICO NACIONAL
25 DE MAYO 658
BUENOS AIRES, ARGENTINA

LIBRARY, CSIRO DIV.
ATMOSPHERIC PHYSICS
STATION STREET
ASPENDALE, 3195
VICTORIA, AUSTRALIA

LIBRARIAN
METEOROLOGY DEPT.
UNIVERSITY OF MELBOURNE
PARKVILLE, VICTORIA 3052
AUSTRALIA

BUREAU OF METEOROLOGY
ATTN: LIBRARY
BOX 1289K, GPO
MELBOURNE, VIC, 3001
AUSTRALIA

AUSTRALIAN NUMERICAL METEOROLOGY
RESEARCH CENTER
ATTN: DR. R. L. HUGHES
P.O. BOX 5089A
MELBOURNE VICTORIA, 3001
AUSTRALIA

DEPT. OF GEOGRAPHY
JAMES COOK UNIVERSITY OF
NORTH QUEENSLAND
TOWNSVILLE Q4811
AUSTRALIA

RAN RESEARCH LABORATORY
ATTN: DR. IAN S.F. JONES
P.O. BOX 706
DARLINGHURST NSW 2010
AUSTRALIA

CHAIRMAN
DEPT. OF METEOROLOGY
MCGILL UNIVERSITY
805 SHERBROOKE ST. W.
MONTREAL, QUEBEC
CANADA H3A2K6

LIBRARY
ATMOS. ENVIRONMENT SERVICE
4905 DUFFERIN STREET
DOWNSVIEW M3H 5T4, ONTARIO
CANADA

DIRECTOR OF METEOROLOGY &
OCEANOGRAPHY
NATIONAL DEFENSE HDQ
OTTAWA, ONTARIO, K1A 0K2
CANADA

INSTITUTE OF OCEANOGRAPHY
UNIV. OF BRITISH COLUMBIA
VANCOUVER BC, CANADA V6T-1W5

METOC CENTRE
MARITIME FORCES PACIFIC HDQ
FORCES MAIL OFFICE
VICTORIA, BRITISH COLUMBIA
VOS-1B0 CANADA

DEFENCE RSCH ESTABLISHMENT
PACIFIC
ATTN: DIRECTOR-GENERAL
FORCES MAIL OFFICE
VICTORIA, BRITISH COLUMBIA
VOX 1B0, CANADA

PACIFIC BIOLOGICAL STATION
LIBRARY, FISHERIES & OCEANS
NANAIMO, BRITISH COLUMBIA
CANADA V9R 5K6

INSTITUTE OF OCEANOGRAPHY
ATTN: DIRECTOR
DALHOUSIE UNIVERSITY
HALIFAX, NOVA SCOTIA, B3H-4J1
CANADA

INSTITUT FOR TEORETISK
METEOROLOGI
HARALDSGADE 6
DK-2200 KOBENHAVN N
DENMARK

INTERNATIONAL COUNCIL FOR
SEA EXPLORATION
ATTN: GENERAL SECRETARY
CHARLOTTENLUND SLOT
DK-2920 CHARLOTTENLUND
DENMARK

METEOROLOGICAL OFFICE LIBRARY
LONDON ROAD
BRACKNELL, BERKSHIRE
RG 12 2SZ
ENGLAND

LIBRARY
INSTITUTE OF OCEANOGRAPHIC SCI.
ATTN: DIRECTOR
WORMLEY, GODALMING
SURRY GU8 5UB, ENGLAND

DEPT. OF METEOROLOGY
UNIVERSITY OF READING
2 EARLYGATE, WHITEKNIGHTS
READING RG6 2AU
ENGLAND

EUROPEAN CENTRE FOR MEDIUM
RANGE WEATHER FORECASTS
SHINFIELD PARK, READING
BERKSHIRE RG2 9AX, ENGLAND

LIBRARY
FINNISH METEOROLOGICAL
INSTITUTE, BOX 503
SF-00101 HELSINKI 10
FINLAND

METEOROLOGIE NATIONALE
SMM/DOCUMENTATION
2, AVENUE RAPP
75340 PARIS CEDEX 07
FRANCE

SERVICE HYDROGRAPHIQUE ET
OCEANOGRAPHIQUE DE LA MARINE
ETABLISSEMENT PRINCIPAL
CENTRE DE DOCUMENTATION
RUE DU CHATELLIER, B.P. 426
29275 - BREST CEDEX
FRANCE

EUROPEAN SPACE AGENCY
METEOROLOGICAL PROGRAM DEPT.
TOULOUSE, FRANCE
ATTN: DR. J. P. ANTIKIDES

DIRECTION DE LA METEOROLOGIE
ATTN: J. DETTWILLER
77 RUE DE SEVRES
92106 BOULOGNE-BILLANCOURT CEDEX
FRANCE

INSTITUT FUR MEERESKUNDE DER
UNIVERSITAT HAMBURG
ATTN: DIRECTOR
HEIMHUEDERSTRASSE 71
2000 HAMBURG 13
FEDERAL REPUBLIC OF GERMANY

HEAD
DATA PROCESSING SECTION
GERMAN MILITARY GEOPHYSICAL OFFICE
MONT ROYAL, D-5580
TRABEAU-TRARBACH
FEDERAL REPUBLIC OF GERMANY

DEUTSCHER HYDROGRAPHISCHES INSTITUT
ATTN: DIRECTOR
TAUSCHSTELLE
POSTFACH 220
02000 HAMBURG 4
FEDERAL REPUBLIC OF GERMANY

EUROPEAN SPACE AGENCY
EUROPEAN SPACE OPERATIONS CEN.
ATTN: DR. JOHN MORGAN
DARMSTADT
FEDERAL REPUBLIC OF GERMANY

MAX PLANCK INSTITUT FUR CHEMIE
ATTN: DR. R. JAENICKE
POSTFACH 3060
D-65 MAINZ
SAARSTR 23
WEST GERMANY

CHIEF HYDROMETEOROLOGICAL OFFICER
HYDROMETEOROLOGICAL DIV.
MINISTRY OF WORKS & COMMUNICATIONS
P.O. BOX 26
GEORGETOWN, GUYANA
SOUTH AMERICA

DIRECTOR
ROYAL OBSERVATORY
NATHAN ROAD, KOWLOON
HONG KONG, B.C.C.

THE DIRECTOR
INDIAN INSTITUTE OF TROPICAL
METEOROLOGY
RAMDURG HOUSE
PUNE 411-005
INDIA

DEPT. OF METEOROLOGY
ANDHRA UNIVERSITY
WALT AIR, INDIA 530-003

DIRECTOR
METEOROLOGICAL & GEOPHY. SERV.
C/O DJALAN ARIEF RACHMAN HAKIM 3
DJAKARTA, INDONESIA

LIBRARY
IRISH METEOROLOGICAL SERVICE
GLASNEVIN HILL
DUBLIN 9, IRELAND

DIRECTOR
ISRAEL METEOROLOGICAL SERVICE
P.O. BOX 25
BET DAGEN 50200, ISRAEL

CONSIGLIO NAZIONALE DELLE RICERCHE
ISTITUTO TALASSOGRAFICO DI TRIESTE
VIALE R. GESSI 2 - 34123 TRIESTE
ITALY

ISTITUTO UNIVERSITARIO NAVALE
FACOLTA DI SCIENZE NAUTICHE
ISTITUTO DI METEOROLOGIA E
OCEANOGRAFIA
80133 NAPOLI - VIA AMM
ACTON, 38 ITALY

OCEAN RESEARCH INSTITUTE LIBRARY
UNIVERSITY OF TOKYO
15-1, 1-CHOME
MINAMIDAI, NAKANO-KU
TOKYO, JAPAN

MARITIME METEOROLOGY DIVISION
JAPAN METEOROLOGICAL AGENCY
OTE-MACHI 1-3-4 CHIYODA-KU
TOKYO, JAPAN

JAPAN METEOROLOGICAL AGENCY
3-4, OTEMACHI 1-CHOME, CHIYODA-KU
TOKYO 100, JAPAN

METEOROLOGICAL INSTITUTE
FACULTY OF SCIENCE
KYOTO UNIVERSITY
ATTN: DR. R. YAMAMOTO
SAKYO, KYOTO 606
JAPAN

DIRECTOR GENERAL
MALAYSIAN METEOROLOGICAL SERV.
JALAN SULTAN
PETALING JAYA
SELANGOR, WEST MALAYSIA

INSTITUTO DE GEOFISICA
U.N.A.M. BIBLIOTECA
TORRE DE CIENCIAS, 3ER PISO
CIUDAD UNIVERSITARIA
MEXICO 20, D.F.

KONINKLIJK NEDERLANDS
METEOROLOGISCH INSTITUUT
POSTBUS 201
3730 AE DEBILT, NETHERLANDS

PHYSICS LAB OF THE NATIONAL
DEFENCE RSCH ORGANIZATION TNO
P.O. BOX 96864
2509 JG
THE HAGUE, NETHERLANDS

BUREAU HYDROGRAFIE DER
KONINKLIJKE MARINE
AFD MILOC/METEO
BADHUISWEG 171
DEN HAAG, NETHERLANDS

THE LIBRARIAN
NEW ZEALAND OCEANOGRAPHIC
INSTITUTE
P.O. BOX 12-346
WELLINGTON NORTH, NEW ZEALAND

DEPT. OF METEOROLOGY
COLLEGE OF ARTS & SCIENCES
UNIV. OF THE PHILIPPINES
DILMAN, QUEZON CITY 3004
PHILIPPINES

THE LIBRARIAN
PHILIPPINE ATMOSPHERIC
GEOPHYSICAL & ASTRONOMICAL
SERVS. ADMIN (PAGASA)
1424 QUEZON AVE.
QUEZON CITY, PHILIPPINES

DIRECTOR
TYPHOON MODERATION RSCH &
DEVELOPMENT OFFICE PAGASA
MINISTRY OF NATIONAL DEFENSE
1424 QUEZON AVE.
QUEZON CITY, PHILIPPINES

NATIONAL RESEARCH INSTITUTE
FOR OCEANOLOGY
COUNCIL FOR SCIENTIFIC &
INDUSTRIAL RESEARCH
P.O. BOX 17001
CONGELLA, 4013,
SOUTH AFRICA

INSTITUTE OF OCEANOGRAPHY
UNIVERSITY OF CAPE TOWN
RONDEBOSCH
CAPE TOWN, SOUTH AFRICA

INSTITUTE FOR MARITIME TECH
P.O. BOX 181
SIMONSTOWN, 7995
REPUBLIC OF AFRICA

LIBRARY
UNIV. OF STOCKHOLM
DEPT. OF METEOROLOGY
ARRHENIUS LABORATORY
S-106 91 STOCKHOLM, SWEDEN

DIRECTOR
SWEDISH METEOROLOGICAL &
HYDROLOGICAL INSTITUTE
P.O. BOX 923
S-601, 19 NORRKOPING
SWEDEN

CHIEF
ATMOSPHERIC SCIENCES DIV.
WORLD METEOROLOGICAL ORG.
P.O. BOX 5
GENEVA 20
SWITZERLAND

DUDLEY KNOX LIBRARY - RESEARCH REPORTS



5 6853 01078724 5

U196795